Chapter 2

Literature Review

In this chapter, a number of recent studies have been critically analyzed to demonstrate that how the surface polarization or electric field stimulation together with functional properties of piezoelectric biomaterials can synergistically modulate cell functionality or tissue regeneration, in vitro / in vivo. The challenging problem of processing the compositionally tailored bioceramics is emphasized in particular reference to (Na, K)NbO_3, an implantable biomaterial with the most attractive combination of piezoresponsive properties. In addition, an overview of bacterial infection in implants and various stimuli to inhibit bacterial infection such as, external electrical stimulation, magnetic field stimulation and surface charge potential has also been discussed.

2.1 Introduction

Bioelectrical cues in natural living bone, such as, piezoelectricity, pyroelectricity and ferroelectricity, etc. have been reported as some of the key factors in regulating metabolic activities like growth, structural remodeling as well as fracture healing [1, 2, 3, 4, 5]. The non-centrosymmetry of the collagen molecule has been suggested as the primary reason for the bioelectricity in living bone [1, 2, 5, 6, 7, 8]. The endogenous electric field of living bone also helps in governing the cell metabolism, such as, growth and proliferation, differentiation, motility, etc [9]. For example, human tibia generates a piezoelectric potential of about 300 μV during walking [10]. The application of physiological compressive loads increases the negative charges due to piezoelectric potential in bone [6, 11]. These negative charges promote the functionality of osteoblast cells and consequently, enhance bone regeneration [6]. However, low mechanical pressure results in reduced neo-bone formation

as compared to higher pressure [12, 13]. The fractured region of living bone becomes more electronegative than the other regions [12, 14]. As mentioned above, the generation of these negative charges promotes the activity of osteoblast cells, which help in matrix mineralization at the fractured site [6, 11]. It can, therefore, be suggested that piezoelectric stimulation plays an important role in controlled bone regeneration. The piezoelectric collagen in bone also develops streaming potential under stress, which results in the reduction of hydraulic permeability as well as an increase in stiffness [15]. Apart from piezoelectricity, the biological response of hard tissues can also be improved by direct electrical stimulation [16, 17, 18, 19, 20, 21, 22, 23, 24, 25, 26].

The stress induced potential in piezo-bioceramics and piezo-biopolymers augments bone metabolism [27, 28, 29, 30, 31, 32]. Piezoelectric bioceramics have already been demonstrated as sources of *in vivo* energy for biosensors and pacemakers [33, 34]. Piezo-bioceramics/ biopolymers develop surface electrical charges under the application of external stress, similar to bone [Fig. 2.1 (A) and (B)] [35, 36, 37]. The polarized piezoelectric surfaces are reported to improve the osteogenic performance of natural bone [38, 39, 40, 41, 42]. Piezoelectric implants can potentially promote bone fracture repair [40, 42]. The implantation of piezoelectric scaffolds at the damaged site of the bone defect, develop stress generated electrical stimuli through physiological loads [Fig. 2.1 (C)] [43]. Such hyperpolarization activates voltage-gated calcium channels of the cell membrane [40]. The intracellular Ca^{2+} ions play an important role in cell proliferation [44]. It can, therefore, be inferred that piezoelectric biocompatible scaffolds result in an early repair of damaged tissue as compared to their non-piezoelectric counterparts [40]. For example, Liu et al. [45] compared the osseointegration of positively polarized $BiFeO_3$ (+BFO) membrane – strontium

titanate (STO), negatively polarized BFO membrane – STO implant and non-polarized STO implant by the fixation in the rat femur. A built in or integral electric field [Fig. 2.1 (D)] develops at the interface of oppositely charged +BFO-STO (+75 mV) and electronegative bone defect surface (−52 to 87 mV) [45, 46], which consequently promote more osseointegration as compared to −BFO-STO and non-polarized STO surfaces [Fig. 2.1 (E)].

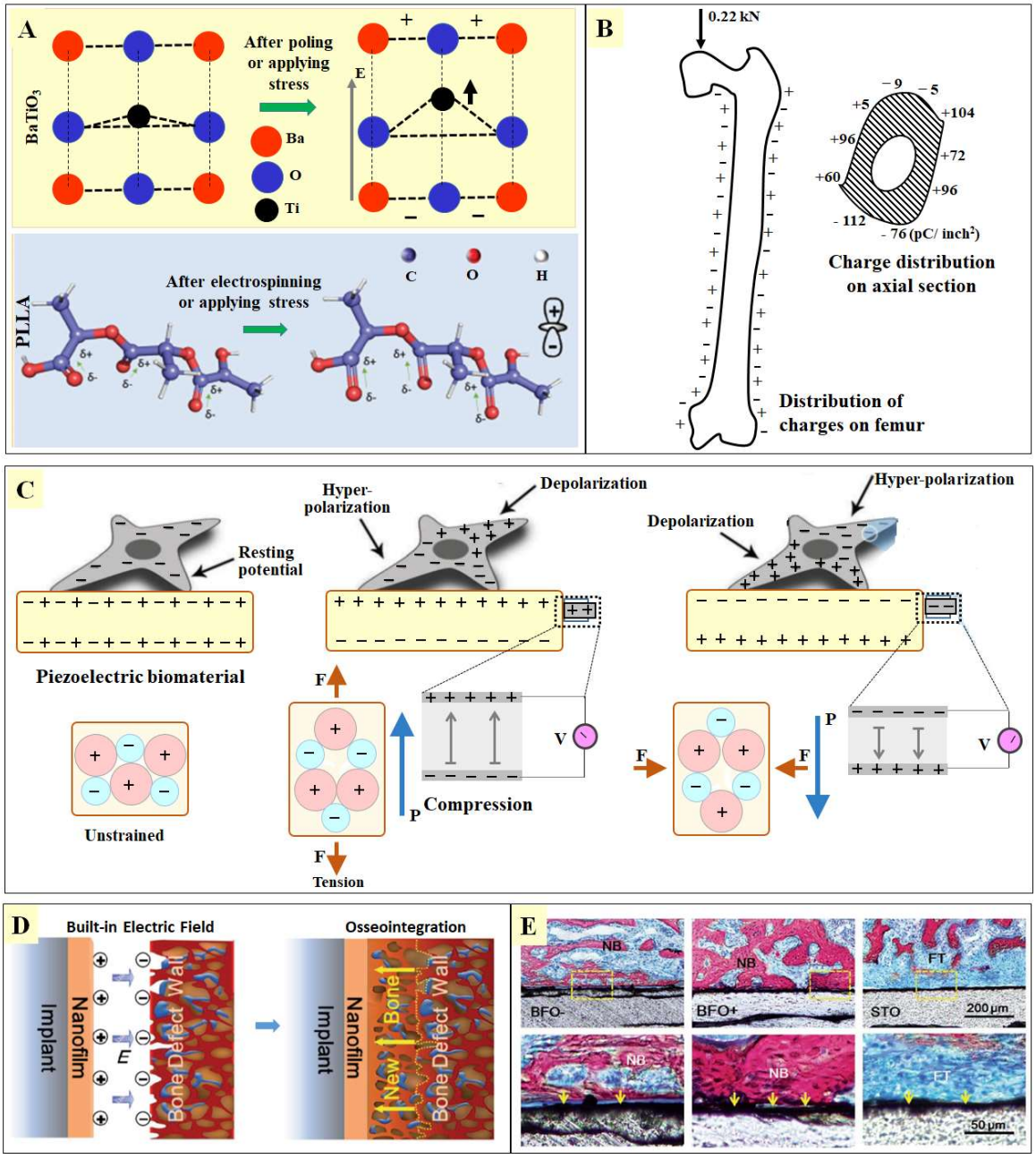

Fig. 2.1. Stress generated electrical charges in natural bone and piezoelectric biomaterials induced endogenous cellular potential and bone formation. (A) Schematic demonstration of the generation of aligned dipoles or surface charge on piezoelectric ceramic ($BaTiO_3$) and polymer (PLLA) with the application of mechanical stress, similar to human bone (Reproduced with the permission from publisher, Ref. [35]). (B) Stress generated surface

electrical charge on the circumference of human femur (Reproduced with the permission from publisher, Ref. [37]). (C) Schematic illustration of the generation of surface electrical charge on strained piezoelectric material and resulting hyper-polarization/ depolarization of cellular membrane (Reproduced with the permission from publisher, Ref. [43]). (D) Schematic representation of built-in electric field between positively charged nanocomposite and negatively charged bone wall, which enhances the osseointegration (Reproduced with the permission from publisher, Ref. [45]). (E) Histological evidences demonstrating significant neobone formation on the positively charged implant, when compared to negatively charged and uncharged implant (Yellow dotted block: implant-tissue interface, NB: nascent bone, FT: fibrous tissue, BFO: $BiFeO_3$, STO: $SrTiO_3$) (Reproduced with the permission from publisher, Ref. [45].

Figs. 2.2 (A), (B) and (C) illustrate the piezoelectric voltage generation from human bone during our routine activity [47, 48, 49]. For this purpose, piezoelectric sensors were embedded with skin, which was then subjected to stress during bend-release of fingers and elbow, during running etc. Positive and negative voltages were produced during bending and releasing of fingers, elbow and knee. Wang et al. [50] experimentally evaluated stress generated electrical potential from the implanted piezoelectric P(VDF-TrFE) scaffold during daily activity of Sprague Dawley rat [Fig. 2.2 (D)]. At the pulling condition of rat's leg, the peak output current and voltage from the strained implanted piezoelectric scaffold were recorded as 6 nA and 6 mV, respectively. Therefore, it can be suggested that the piezoelectric scaffold, implanted in the wounded site, generates electrical potential under physiological loads. This further stimulates osteoblastic activity and consequently, promotes bone regeneration in the wounded region.

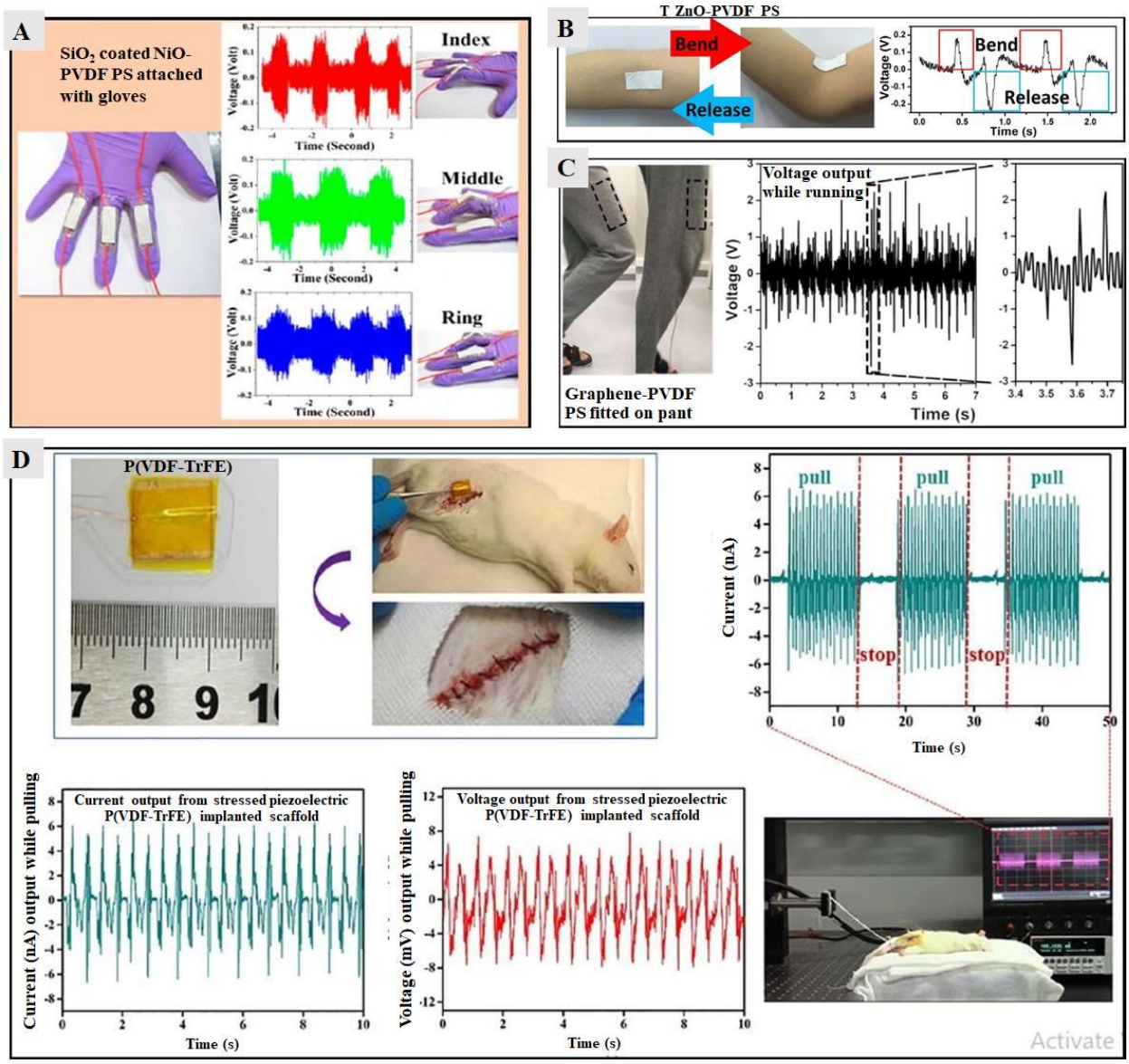

Fig. 2.2. Piezoelectric potential generated from natural bone during regular physiological activity. [(A), (B) and (C)] PVDF based piezoelectric sensors (PS) as detectors of human activity in terms of piezoelectricity induced voltage output. [D] P(VDF-TrFE) based piezo-polymers (nanogenerator) implanted in the thigh of Sprague Dawley rat, mimicking piezoelectric potential generation during the regular activity. (A) PS nanocomposite, fabricated with PVDF/ SiO_2 coated NiO assembled with gloves to determine the piezoelectric voltage output variation during stretching and bending movement of index, middle and ring

fingers (Reproduced with the permission from publisher, Ref. [47]). (B) A PS nanocomposite with tetrapod ZnO/ PVDF/ polyester fabric, attached with elbow, to evaluate the amount of voltage output during bending and release (Reproduced with the permission from publisher, Ref. [48]). (C) A PS fabricated with PVDF/ graphene in polyester fabric attached with marked region to determine the voltage output variation during running (Reproduced with the permission from publisher, Ref. [49]). (D) Electrospun P(VDF-TrFE) nanoscaffold implanted in the thigh of Sprague Dawley rat. The leg of rat was pulled up and released through a motor (bottom-right) and resulting variation in current output are shown (top-right) during pulling and releasing. The current and voltage output are also shown in bottom-left and bottom-middle graph, respectively in the pulling condition of rat's leg (Reproduced with the permission from publisher, Ref. [50]).

Against the above backdrop, the potentiality of various piezoelectric bioceramics and biopolymers in mimicking electro-mechanical response of living bone has been revealed. Towards this end, the processing-related challenges to meet the desired piezoresponsive property combination have been discussed along with the possible combinations of remedies. In addition, the advantageous effects of polarized piezoelectric substrates in augmenting the biocompatibility have been discussed objectively.

NKN and $BaTiO_3$ possess ferroelectricity at a temperature lower than the Curie temperature, as represented in Figs. 2.3 (a) and (b), respectively. In $Na_{0.5}K_{0.5}NbO_3$ ceramics, temperature dependent ferroelectric phase transformations occur from cubic to tetragonal (at ~ 420 °C) to monoclinic / orthorhombic (at ~ 210 °C) to rhombohedral (≤ - 160 °C) phases [51, 52, 53]. However, in $BaTiO_3$ ceramics, ferroelectric phase transformations take place from tetragonal

(130 to 5 °C) to orthorhombic (5 to - 90 °C) to rhombohedral (≤ - 90 °C) phases. Overall, NKN and $BaTiO_3$ exhibit ferroelectric phase at room temperature [54].

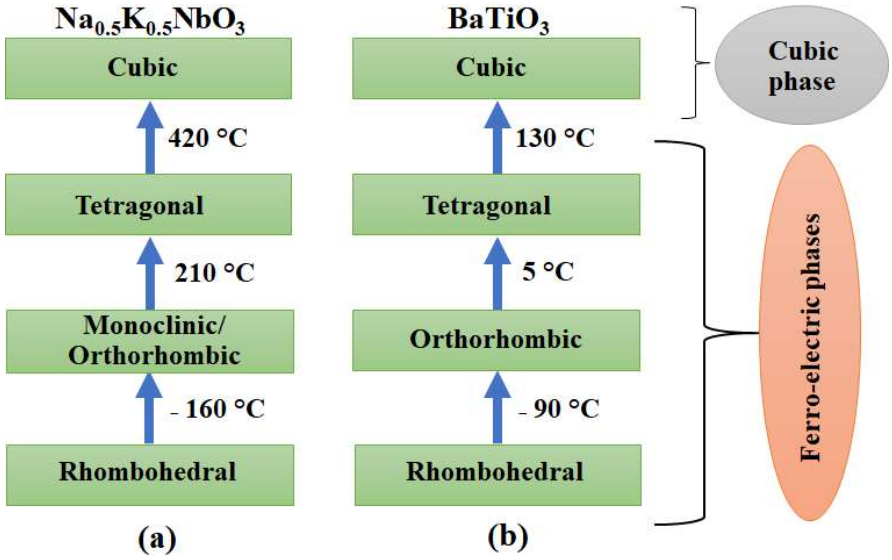

Fig. 2.3. Schematic illustrating the temperature dependent phase transformations (a) In $Na_{0.5}K_{0.5}NbO_3$ [51, 52, 53] and (b) In $BaTiO_3$ ceramics [54].

2.2. Piezoelectric biomaterials

Among various biomaterials, piezoelectric bioceramics, such as, sodium potassium niobate ($Na_xK_yNbO_3$, where, $0 \leq x \leq 0.8$; $0.2 \leq y \leq 1$; NKN) [55] or NKN-based ceramics [56, 57], $BaTiO_3$ [5, 38, 58, 59, 60], lithium sodium potassium niobate [61, 62, 63], $LiNbO_3$ [64, 65], $MgSiO_3$ [66, 67, 68], $KNbO_3$ [69], ZnO [44], boron nitride [70], bismuth ferrite ($BiFeO_3$) [71] are reported to demonstrate reasonable potentiality to be prospective electroactive prosthetic implants. Similar examples from the class of piezoelectric biopolymers include polyvinylidene fluoride (PVDF) [42], poly-L-lactic acid (PLLA) [72], polyhydroxybutyrate (PHB) [73], polyamides (Nylons, peptides, etc.) [74], polysaccharides (cellulose, chitosan, etc.) [75, 76, 77], collagen [78], etc. The dielectric, piezoelectric, ferroelectric, pyroelectric and electromechanical properties of the above mentioned piezoelectric bioceramics/

biopolymers are summarized in Table 2.1 [7, 8, 29, 63, 65, 79, 80, 81, 82, 83, 84, 85, 86, 87, 88, 89, 90, 91, 92, 93, 94, 95, 96, 97, 98, 99, 100, 101, 102, 103, 104, 105, 106, 107, 108, 109, 110, 111, 112, 113, 114, 115, 116, 117, 118, 119, 120, 121, 122, 123, 124, 125, 126, 127, 128].

Table 2.1. A comparison of dielectric constants (ε_r), piezoelectric strain coefficients (d_{33}), mechanical quality factors (Q_m), remnant polarization (P_r), electromechanical coupling coefficients (k_P) and pyroelectric coefficients (p) of various piezoelectric biomaterials with those of the natural bone.

Piezoelectric Biomaterials	**ε_r (at 1-100 kHz)**	**d_{33} (pC/N)**	**(Q_m)**	**P_r ($\mu C/cm^2$)**	**k_p (%)**	**(p) ($\mu C/m^2K$)**	**Ref.**
$Na_{.5}K_{.5}NbO_3$	657	160	240	31.4	44	-	[83, 84]
Barium titanate ($BaTiO_3$)	1135	191	32	12.6	35	200	[85, 86, 87, 88, 89]
$Li_{0.06}(Na_{0.5}K_{0.5})_{0.94}NbO_3$	722.4	124	-	16.8	30.63	-	[63, 90]
Lithium niobate ($LiNbO_3$)	62	23	-	-	-	103.9	[65, 91, 92]
Magnesium silicate ($MgSiO_3$)	-	- 1.74 (d_{31})	-	-	-	-	[93]
Potassium niobate ($KNbO_3$)	394	91.7	325	-	28	93	[94, 95]
Zinc oxide (ZnO)	12.27	12.4	-	16.31	48 (k_{33})	9.4	[89, 97, 98, 99]
Boron nitride (BN)	2 - 4	31.2 (d_{31})	-	-	-	-	[100, 101]
Polyvinylidene fluoride (PVDF)	6 - 12	34	17.2	13	20 (k_{33})	41	[102, 103, 104, 105, 106, 107, 108]
P(VDF-TrFE)	18	38	-	9.9	29 (k_{33})	50	[103, 109, 110, 111, 112, 113]

Poly-L-lactic acid (PLLA)	3 - 4	9.82 (d_{14})	30.3	-	-	-	[29, 114, 115]
Polyhydroxybutyrate (PHB)	2 - 3.5	1.6-2 (d_{14})	-	-	-	-	[29, 116, 117]
Polyamide	4 - 5	4 (d_{31})	8.5	5.6 - 8.6	11	5	[29, 113, 118, 119, 120, 121]
Collagen	2.6	0.2 - 2 (d_{14})	-	0.29	-	0.12 - 0.37 @ 40 °C	[122, 123, 124, 125]
Chitosan	3.94	0.2 - 1.5 (d_{14})	-	0.178	-	7	[122, 123, 126, 127, 128]
Human bone	9.2	7.50 - 9	-	0.00068	-	0.0036 ± 0.0021	[7, 8, 79, 80, 81, 82, 96]

Among various piezoelectric ceramics, $Na_{.5}K_{.5}NbO_3$ and $BaTiO_3$ exhibit comparatively higher piezoelectric and electrical properties. PVDF shows the best piezoelectric and electrical properties among mentioned piezoelectric polymers. Therefore, such piezoelectric ceramic and polymer can be suggested as potential candidate for orthopedic applications.

The piezoelectricity of the above materials [Table 2.1] is associated with their non-centrosymmetric structures. On the basis of the degree of symmetry or orientation, crystals can be classified into 32 crystal classes [Fig. 2.4] [129, 130]. Among 32 crystal classes, 21 classes possess non-centrosymmetric structures. Of these, one belongs to combined cubic symmetry and does not possess piezoelectricity, whereas, remaining 20 crystal classes exhibit piezoelectric phenomena. 10 crystal classes, among these 20 non-centrosymmetric classes, develop polarization only by the application of mechanical stress and the remaining 10 crystal classes possess spontaneous polarization i.e., they possess piezoelectricity as well

as pyroelectricity. A subgroup of these crystal classes demonstrates reversible spontaneous polarization which defines the ferroelectric behavior [129, 130].

As far as piezoelectric properties are concerned, NKN-based ceramics have been demonstrated among the best candidates, because of their reasonable piezoelectric strain coefficient (d_{33} = 260 pC/N), mechanical quality factor (240), high electromechanical coupling coefficient (k_{33} = 53 %, k_P = 48 %), and high Curie temperature (420°C) as well as relatively lower density (4.51 g/cm^3) as compared to other piezoelectric biocompatible materials [83, 131, 132, 133]. NKN has been patented as a potential biocompatible implant material, as it supports the growth of human monocytes [55]. $BaTiO_3$ is another piezoelectric candidate with proven biocompatibility, *in vivo*. It has been demonstrated that $BaTiO_3$ promotes osteogenesis in dog femur bone [38, 58]. Below its Curie temperature (T_c = 130 °C), $BaTiO_3$ possesses a polar asymmetric structure that imparts piezoelectricity [39, 134]. $MgSiO_3$, with an asymmetric tetragonal structure, has been reported to be a good biocompatible piezoelectric substitute for bone, as testified by various *in vitro* and *in vivo* studies [66, 68, 135, 136].

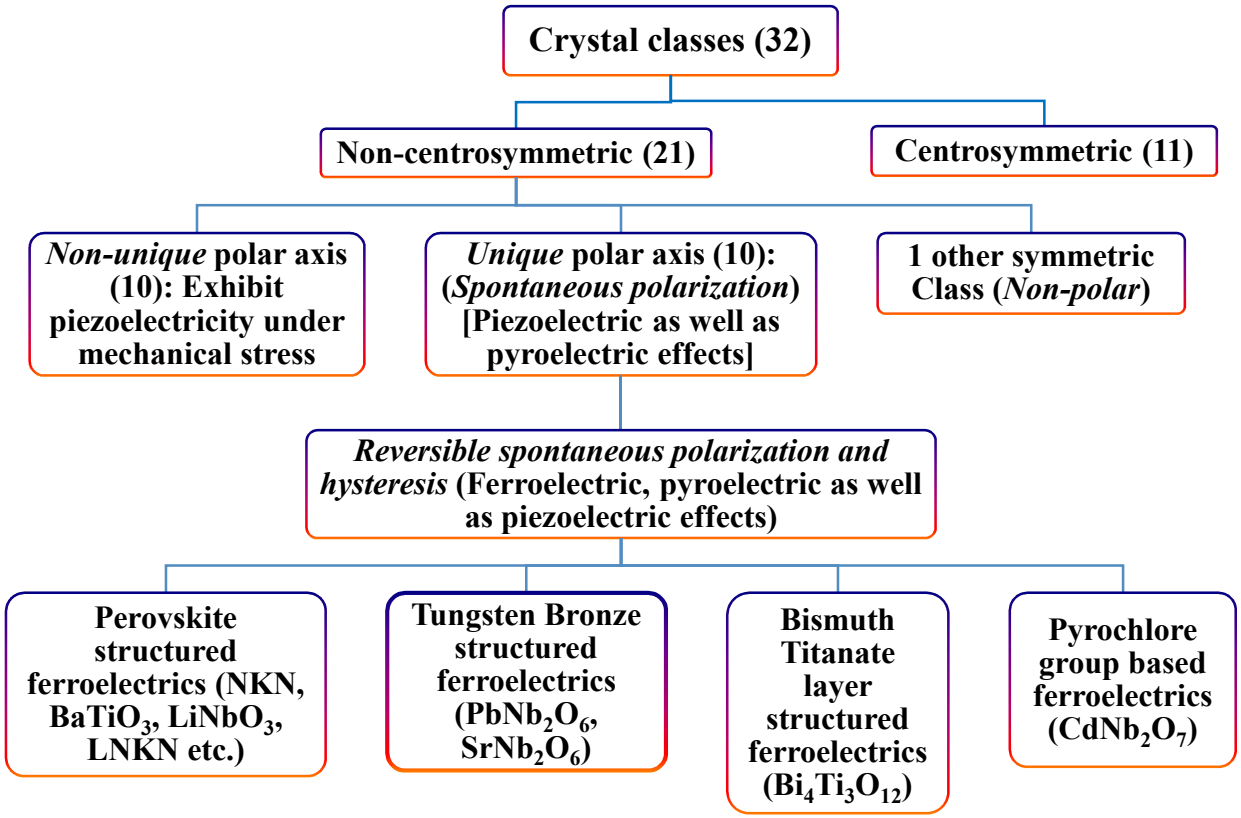

Fig. 2.4. Classification of various crystal classes on the basis of the center of symmetry with reference to piezoelectricity, pyroelectricity and ferroelectricity (adapted from refs. [129] and [130]).

$LiNbO_3$ is another piezoelectric material, which has been suggested as a potential alternative for bone prosthesis [64, 65, 137]. $LiNbO_3$ possesses admirable ferroelectric (spontaneous polarization; p_s = 78 μC/ cm^2), pyroelectric (P = 103.9 μC/m^2°K) and piezoelectric (d_{33} = 23 pC/N) properties [65, 91, 137]. Piezoelectric $KNbO_3$ is currently being used as a bio-probe for disease diagnosis and could be another alternative as an electroactive bone substitute [138, 139]. ZnO is another ceramic with reasonable piezoelectric (d_{33} = 12.4 pC/N) [98], pyroelectric (9.4 μC/m^2K) [89] and dielectric (ε = 12.27) [98] potentials. It also has the ability to generate piezoelectric potential, which results in enhanced cellular functionality and

subsequently, promotes osteogenesis [44]. The piezoelectric boron nitride (BN) nanotubes, in its pristine as well as composite forms, have been reported to promote the proliferation and differentiation of mesenchymal stem cells [70]. Piezoelectric natural (proteins, polysaccharides, etc.) / synthetic (PVDF, PLLA, PHB, etc.) biopolymers are another class of emerging materials, that can be utilized for the regeneration of soft as well as hard tissues [27, 29, 75, 78].

Piezo-bioceramics and piezo-biopolymers are emerging biomaterials as next generation orthopedic implants. However, a number of processing concerns is to be addressed in synthesizing the consolidated stoichiometric composition of the above mentioned piezoelectric ceramics. For example, the volatilization of alkali elements (Na, K) restricts the high temperature processing and consequently, the densification of NKN-based ceramics by conventional processing techniques [131, 140, 141, 142, 143]. To address such processing concerns, a number of approaches, such as use of sintering aids (to reduce the sintering temperature) [144, 145, 146, 147], reduced atmosphere sintering [148, 149], advanced sintering routes, viz. cold isostatic pressing [62], hot pressing [150], hot isostatic pressing [151], spark plasma sintering [152], additive engineering [153, 154, 155, 156] are being investigated.

2.3. Processing-related challenges for piezoelectric NKN-based ceramics system

$Na_xK_{(1-x)}NbO_3$ is a solid solution of ferroelectric $KNbO_3$ and anti-ferroelectric $NaNbO_3$ [Fig. 2.5 (a)] [51, 52]. As illustrated in Fig. 2.5 (a), three morphotropic phase boundaries (MPB) occur at $NaNbO_3$ proportions of 52.5, 67.5 and 82.5 mol. %, respectively [157]. The highest value of the piezoelectric strain coefficient obtained at MPB, which corresponds to the composition, x = 0.5 [52, 157, 158, 159]. Below its Curie temperature (420 °C), three

ferroelectric polymorphs, namely tetragonal, monoclinic / orthorhombic and rhombohedral exist. The polymorphic phase transitions (PPT) from rhombohedral to monoclinic / orthorhombic to tetragonal occur at temperatures of - 160 °C and 200 °C, respectively [Fig. 2.5 (a)] [51, 52, 53]. The PPT in NKN depends on compositions of the precursors as well as temperature [Figs. 2.5 (a) and (b)] [160, 161, 162, 163]. The piezoelectric properties of NKN can be improved by stabilizing the high temperature (200 °C) tetragonal phase at room temperature. The room temperature tetragonal phase in NKN can be established with the doping of Li (7 mol. %) [164], $LiTaO_3$ (5 - 6 mol. %) [153, 160], $LiNbO_3$ (5 - 7 mol. %) [154], $LiSbO_3$ (5.2 mol. %) [161] etc. in NKN matrix. Figs. 2.5 (b) and (c) distinguish the physical significance of PPT and MPB in NKN. As the tetragonal to monoclinic / orthorhombic phase transition temperature can be shifted to room temperature by compositional modifications in NKN, PPT can be suggested to be dependent on composition, as well. However, MPB is dependent on the composition only [165]. PPT is less preferable as compared to MPB due to temperature-dependent fluctuations in dielectric and piezoelectric properties [166, 167]. At room temperature, NKN unit cell is described as the orthorhombic phase, while its primary perovskite cell (ABO_3) shows monoclinic symmetry [157].

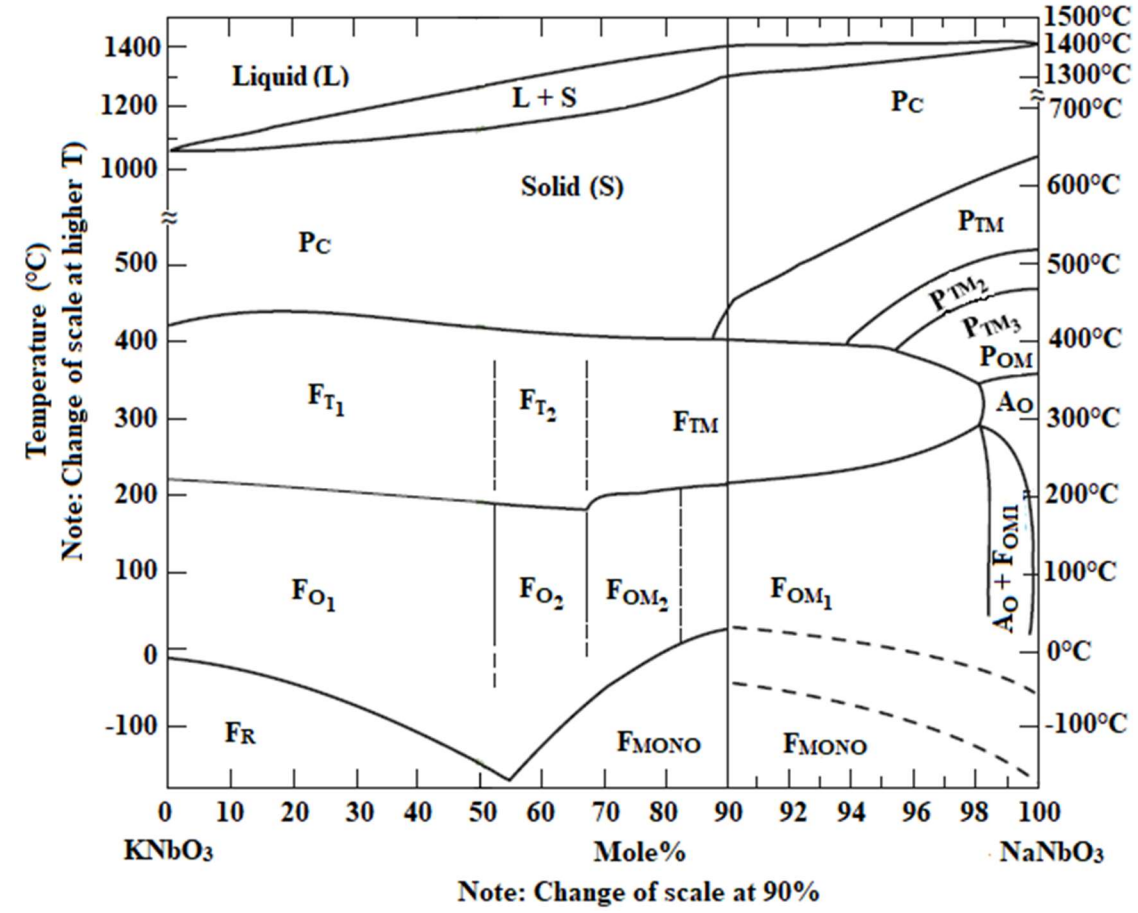

(a)

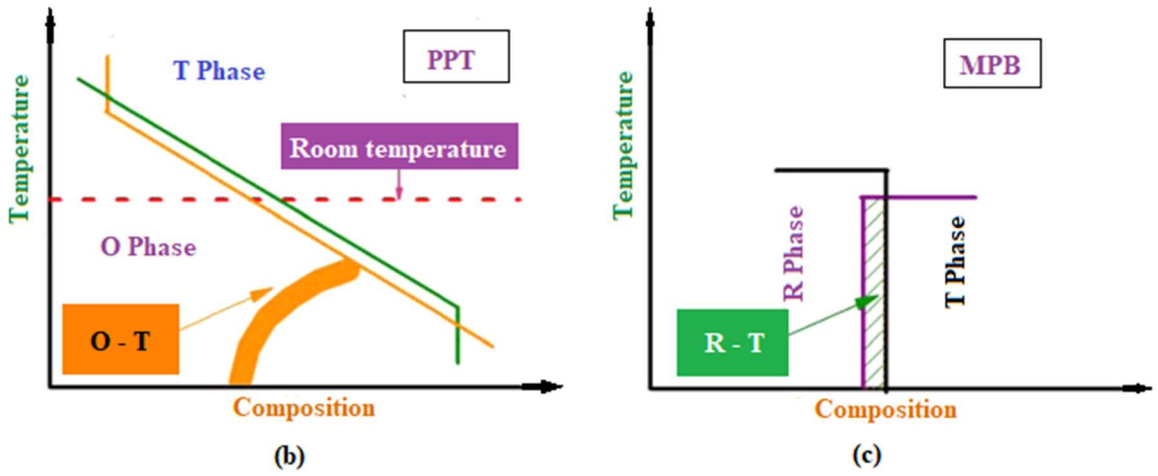

Fig. 2.5 (a). Phase diagram of $KNbO_3$-$NaNbO_3$ solid solution, where P and F denote the paraelectric and ferroelectric phases, respectively. R, O, T and C indicate rhombohedral, monoclinic / orthorhombic, tetragonal and cubic phases, respectively. In $Na_xK_{1-x}NbO_3$, the

morphotropic phase boundary (MPB) at x = 0.5 distinguishes two orthorhombic and two tetragonal phases. Below Curie temperature, polymorphs like tetragonal - monoclinic / orthorhombic and monoclinic / orthorhombic - rhombohedral coexist at about 200 °C and -160 °C, respectively, (Reproduced with the permission from publisher, Ref. [52]). (b) Polymorphic phase transformation (PPT): tetragonal to monoclinic / orthorhombic (polymorphs) phase transformation temperature of NKN can be shifted to room temperature by chemical modification, indicating the dependency of PPT on composition as well as temperature, (c) Morphotropic phase boundary (MPB): Coexistence of rhombohedral and tetragonal phases at a certain composition (Reproduced with the permission from the publisher, Ref. [165]).

Malice et al. [168] suggested that the number of intermediate reactions takes place between the constituent phases (Na_2CO_3, Nb_2O_5, and K_2CO_3) during the formation of $Na_{0.5}K_{0.5}NbO_3$ ceramics via solid-state synthesis route. During calcination, two raw binary (Na_2CO_3/Nb_2O_5, K_2CO_3/Nb_2O_5) phases and a tertiary raw ($Na_2CO_3/K_2CO_3/Nb_2O_5$) phase reacts, as follows [168],

$$Na_2CO_3 + Nb_2O_5 \xrightarrow{500^\circ C} Na_2Nb_4O_{11}(Non-perovskite\ phase)$$

(2.1)

$$Na_2CO_3 + Na_2Nb_4O_{11} \xrightarrow{700^\circ C} NaNbO_3(Perovskite\ phase)$$

(2.2)

$$K_2CO_3 + Nb_2O_5 \xrightarrow{600^\circ C} K_6Nb_{10.88}O_{30} + K_4Nb_6O_{17} + KNbO_3(Perovskite\ phase)$$

(2.3)

$$Na_2CO_3 + K_2CO_3 + Nb_2O_5 \xrightarrow{600^\circ C} Na_{0.5}K_{0.5}NbO_3(Perovskite\ phase) + (K,Na)_2Nb_4O_{11}$$

(2.4)

The calcination temperature for NKN has been suggested to be in the range of 750 °C to 950 °C [83, 131, 132, 168, 169, 170, 171, 172, 173].

The alkali volatilization at the higher temperatures (> 1000 °C) and hygroscopic nature of alkaline carbonate precursors, especially K_2CO_3 are the primary concerns associated with the processing of stoichiometric NKN-based ceramics [140, 174]. The melting temperature of $NaNbO_3$ and $KNbO_3$ are about 1420 °C and 1040 °C, respectively [142, 175]. The consolidation, as well as microstructural control during high temperature sintering of NKN-based ceramics is difficult due to their close sintering and solidus temperatures [131, 141, 142, 176]. The solidus and liquidus temperatures for $Na_{0.5}K_{0.5}NbO_3$ are about 1140 ºC and 1280 ºC, respectively [142]. In addition, a difference in diffusion rates of Na and K ions, with K^+ being the slowest diffusing species, retards the formation of stoichiometric NKN [143]. High vapor pressure of alkalis at higher temperatures (~ 990 °C) results in alkali phase reduction in NKN. The difference in equilibrium vapor pressures of K ($P_K = 8\times10^{-3}$ Pa) and Na ($P_{Na} = 3\times10^{-3}$ Pa) has also been suggested as one of the issues in the processing of stoichiometric NKN-based ceramics [177]. Fig. 2.6 represents the key processing concerns in achieving phase pure and dense NKN.

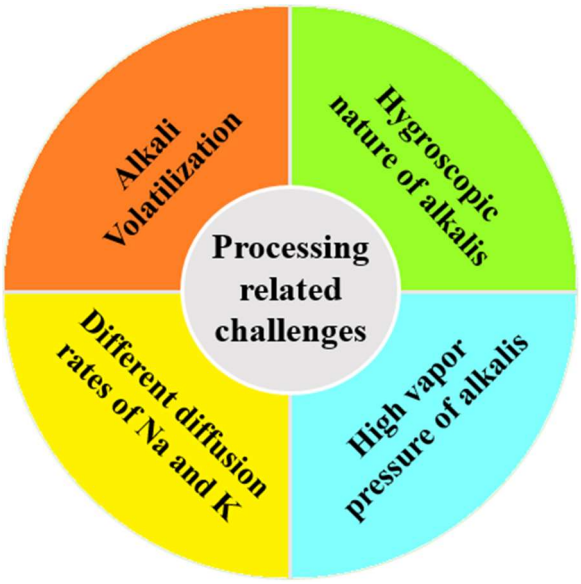

Fig. 2.6. Schematic representing key issues, associated with the processing of stoichiometric NKN [131, 141, 142, 143, 176, 177].

2.4. Addressing the processing concerns for piezoelectric NKN-based ceramics

The alkali volatilization at higher temperatures results in the formation of secondary phases, such as, $K_6Nb_{10.88}O_{30}$, $K_2Nb_4O_{11}$, etc. [178]. The sintering of NKN, above 1000 °C, causes the formation of liquid phase due to the evaporation of Na_2O, which results in higher densification [141]. However, Na_2O evaporation results in the reduction of piezoelectric properties of NKN ceramics [141]. In order to control the evaporation of Na_2O, various sintering aids (low melting point oxides) such as, ZnO doped - CuO (sintering temperature, T_s = 900 °C) [144], V_2O_5 (T_s = 920 °C) [145], (K, Na) - Germanate (T_s = 1000 °C) [146], Li_2O (T_s = 1000 °C) [147] etc. have been incorporated to reduce the sintering temperature of NKN-based ceramics. The addition of 5 mol. % $BaTiO_3$ to the NKN specimen (0.95 $Na_{.5}K_{.5}NbO_3$ - 0.05 $BaTiO_3$) has also been suggested as one of the ways to control Na_2O evaporation [141]. Such modification results in excellent piezoelectric properties (k_P = 36 %, d_{33} = 225 pC/N) at relatively lower sintering temperature of 1060 ºC (2 h) [141].

The consolidation of NKN can also be improved by liquid phase sintering (LPS) [179], where sintering aids with the lower melting point are incorporated in NKN matrix phase to reduce the sintering temperature. It prevents alkali phase reduction, which consequently, enhances the densification of NKN-based ceramics. Therefore, the piezoelectric as well as electrical properties of NKN can be improved either by reducing the sintering temperature below 1000 °C or by controlling the evaporation of Na_2O at higher temperatures (> 1000 °C). The important LPS aids for NKN includes, Cu, Zn, borate and germinate-based compounds [146, 180, 181, 182, 183]. Cu-based sintering aids are $K_4CuNb_8O_{23}$ (0.5 mol. %), $K_{5.4}Cu_{1.3}Ta_{10}O_{29}$ (0.38 mol. %), etc., which enhance the densification (> 97.6 % ρ_{th}) and piezoelectric properties (d_{33} = 180 - 190 pC/N, k_P = 39 - 42 %, Q_m = 1200 - 1400) of NKN-based ceramics, at relatively lower sintering temperatures (1095 - 1120 °C) [180]. The addition of ZnO (1 mol. %) and $K_{1.94}Zn_{1.06}Ta_{5.19}O_{15}$ (0.5 mol. %) has also been reported to provide improved densification (upto 96.3 % ρ_{th}) and piezoelectric properties (d_{33} = 123 - 126 pC/N, k_P = 40 - 42 %, Q_m = 60 - 140) of NKN-based ceramics [181, 182]. Similarly, borate-based sintering aids such as, 0.45 wt. % of borax or $Na_2B_4O_7$. 10 H_2O (ρ_r = 95.5 % ρ_{th}, d_{33} = 131.6 pC/N, k_P = 34.8 %, Q_m = 109) [183] and 1 wt. % of germinate-based K, Na-germinate sintering aids (ρ_r = 95.6 % ρ_{th}, d_{33} = 120 pC/N, k_P = 40 %, Q_m = 77) also contribute to the densification and piezoelectric properties of NKN-based ceramics [146].

Kobayashi et al. [148, 149] suggested that the sintering in reduced oxygen can effectively diminish the possibility of the volatilization of alkalis during the processing of NKN ceramics. Such processing results in relatively high dielectric constant (415.6) and resistivity (2.70 x 10^9 Ω-m**)** in NKN. In reduced atmosphere sintering, the energy for the formation of oxygen vacancies decreases and that of alkali vacancies increases. Consequently, oxygen

vacancy increases and alkali (Na, K) vacancy decreases, which indicates a decrease in alkali volatilization. Alkali volatilization during sintering in air as well as reduced oxygen atmosphere can be represented as [148, 149],

(a) In air atmosphere (p-type conduction),

$$2M_m + O_o(gas) \rightarrow M_2O(gas) + 2V_m^{'} + V_o^{\bullet\bullet} \qquad (2.5)$$

$$2V_m^{'} + V_o^{\bullet\bullet} + \frac{1}{2}O_2 \rightarrow 2V_m^{'} + O_o + 2h^{\bullet} \qquad (2.6)$$

The combination of Eqns. (2.5) and (2.6) yields,

$$2M_m + \frac{1}{2}O_2 \rightarrow M_2O(gas) + 2V_m^{'} + 2h^{\bullet} \textit{ (p-type conduction)} \qquad (2.7)$$

(b) In reduced oxygen atmosphere (n-type conduction),

$$O_o \rightarrow \frac{1}{2}O_2(gas) + V_o^{\bullet\bullet} + 2e' \textit{ (n-type reduction)} \qquad (2.8)$$

where, M, V_m, and V_o indicate alkali metal, vacancies of alkali metal and oxygen, respectively.

2.4.1. Conventional processing routes

A number of efforts have been made to obtain reasonable densification in NKN-based ceramics through an inexpensive conventional sintering route. Egerton et al. [169] fabricated NKN ceramics via solid-state route at various sintering temperatures, ranging from 1050 - 1325 °C, which led to the densification of 94 - 97 % ρ_{th}. Similarly, a relative density of 93.4 - 95.3 % ρ_{th} has been reported for the sintering temperatures, ranging from 1100 - 1115 °C (2 h) [172, 184, 185]. However, densification of 97 - 97.6 % ρ_{th} has been demonstrated for the sintering temperature of 1120 - 1125 °C of NKN, which subsequently, exhibits good piezoelectric response (d_{33} = 120 pC/N) [131, 173]. Zuo et al. [132] reported maximum

densification of 98.4 % ρ_{th} in NKN on reducing the particle size in the nano range (70 nm), prior to conventional sintering (1100 °C, 4h). Similarly, Du et al. [173] suggested that apart from sintering temperature (1120 °C, 2h), heating rate (optimized at 5 °C/ min) is one of the important parameters to provide reasonable densification (97.56 % ρ_{th}) and piezoelectric properties (d_{33} = 120 pC/N and k_P = 40 %). $LiNbO_3$ (7 mol. %) modified NKN ceramic i.e., 0.93 ($Na_{0.5}K_{0.5}NbO_3$) - 0.07 ($LiNbO_3$), possesses excellent piezoelectric properties (d_{33} = 240 pC/N and k_P = 35 %), which was consolidated at 1030 °C, followed by annealing at 1050 °C (i.e., two-step sintering) [186]. However, it has been reported that modification with $LiNbO_3$ as 0.942 ($Na_{0.535}K_{0.480}$) NbO_3 - 0.058 $LiNbO_3$ results in further improvement in piezoelectric properties (d_{33} = 314 pC/N, k_P = 41.2 %), when sintered at approximately similar temperature (1060 °C) [187]. Doping of Li and Ta at alkali and niobium side in NKN i.e., ($Li_{0.04}K_{0.44}Na_{0.52}$) ($Nb_{0.85}Ta_{0.15}$) O_3 and subsequent sintering at 1090 °C, reveals increased densification up to 98 % with good piezoelectric property (d_{33} ~ 206 pC/N) [188]. NKN doped with Ta, Sb, and Li i.e., ($Na_{0.52}$ $K_{0.48-x}$) ($Nb_{1-x-y}Sb_y$) O_3 - $LiTaO_3$ results in excellent piezoelectric properties (d_{33} = 242 - 400 pC/N, k_P = 36 - 54 %), when conventionally sintered in the temperature range of 1060 - 1120 °C for 3 h [189]. $BaTiO_3$ (5 mol. %) modified NKN exhibits high piezoelectric strain coefficient (225 pC/N), while sintered at 1060 °C for 2 h [190]. With the conventional sintering technique, it is difficult to achieve the desirable densification for NKN-based ceramics, which is required for the optimal dielectric and piezoelectric properties. Therefore, advanced processing routes have been adapted.

2.4.2. Advanced processing routes

A number of advanced processing routes have been demonstrated to provide better consolidation and piezoelectric properties in NKN-based ceramics. Hot pressing (1100 °C at

38.61 MPa for 20 min.) was the first non-conventional processing route, wherein comparatively refined microstructure and improved piezoelectric (d_{33} = 160 pC/N) response were observed with highly dense (~ 99 % ρ_{th}) NKN-based ceramic [79]. Similarly, Li modified and hot-pressed [850 – 1150 °C at ~ 7 - 69 MPa for 1 h] (Na, K, Li) NbO_3 has been developed with excellent electromechanical coupling coefficient (k_P = 45 %) along with a very high densification of 98.8 - 99.8 % of ρ_{th} [150]. The issues, associated with the consolidation of NKN-based ceramics have also been suggested to address via cold isostatic pressing (CIP) where, high pressure of about 100 to 200 MPa is applied to obtain highly dense ceramics with improved piezoelectric properties [62, 153, 154, 191]. Wang et al. [62] fabricated 50 % porous $Li_{.6}Na_{.5}K_{.44}NbO_3$ ceramic using CIP at a pressure of 100 MPa, followed by sintering at 1075 °C for 2h. Despite of significant porosity, the CIPed material has been demonstrated to possess reasonable piezoelectric properties (d_{33} = 117 ± 6 pC/N, k_P = 24 ± 3 %). CIPed (200 MPa) NKN-based ceramics, modified with $BaTiO_3$ (2 mol. %, T_s = 1100 - 1250 °C), $LiNbO_3$ (5 to 7 mol. %, T_s = 1040 - 1100 °C), $LiTaO_3$ (5 to 6 mol. %, T_s = 1110 °C) or $SrTiO_3$ (0.5 to 2 %, T_s = 1100 - 1250 °C) have been demonstrated to provide profound densification (97 - 98.4 % ρ_{th}) with reasonable piezoelectric properties (d_{33} = 96 - 235 pC/N, k_P = 29 - 44 %) [Table 2.2] [153, 154, 155, 156]. It has been suggested that such kind of improvement in density occurs due to the increase in grain size. In addition, piezoelectric properties are enhanced due to the formation of MPB at the given composition of additives. Maiwa et al. [151] used hot isostatic pressing at temperature and pressure of 800 °C and 200 MPa (for 1 h, in argon atmosphere), respectively, to obtain NKN-based ceramic with a reasonable dielectric (ε_r = 149) and piezoelectric (d_{33} = 40 pC/N) properties. Wang et al. [133] synthesized $LiTaO_3$ as well as Sb-modified NKN powder i.e., $(Na_{0.52}K_{0.4425})$

$(Nb_{0.8825}Sb_{0.08})\ O_3$ - 0.0375 $LiTaO_3$ or (NKNS-3.75LT) with chemisorption sol-gel technique, where, perovskite structure of NKN was formed at a comparatively lower calcination temperature (at 500 – 600 °C) than the conventional fabrication methods (~ 800 °C). Sol-gel prepared $(Na_{0.52}K_{0.4425})$ $(Nb_{0.8825}Sb_{0.08})\ O_3$ - 0.0375 $LiTaO_3$ exhibits favorable piezoelectric properties (d_{33} ~ 418 pC/N, T_c ~ 257 °C and k_P ~ 54 %) by conventional sintering at 1090 °C. Spark plasma sintering (SPS) is one of the most emerging non-conventional routes of sintering to obtain highly dense (~ 96 to 99.8 % ρ_{th}) NKN-based ceramics, with excellent dielectric (ε_r = 243 - 550) as well as piezoelectric properties (d_{33} ~ 148 - 280 pC/N, k_P ~ 26 - 48 %) [152, 158, 171, 192, 193, 194]. These materials were consolidated under the combined action of high pressure (~ 0.6 GPa), rapid heating (~ 150 °C /min.) and at a comparatively lower sintering temperature (920 – 1100 °C). The reduced sintering temperature suppresses the alkali volatilization in NKN, which has very important consequences as far as the dielectric and piezoelectric properties are concerned. Chemically modified NKN with (8 mol. %) $LiTaO_3$ as well as with Li/Ta/Nb i.e., $(Li_{0.04}K_{0.44}Na_{0.52})$ $(Nb_{0.85}Ta_{0.15})$, consolidated by SPS, exhibit adequate piezoelectric properties (d_{33} = 185 - 243 pC/N, k_P = 44 - 50 %) [Table 2.2] [195, 196, 197, 198]. Table 2.2 summarizes the influence of various sintering techniques on densification, piezoelectric strain coefficient (d_{33}) and electromechanical coupling coefficient (k_P) of NKN/ NKN-based ceramics.

Table 2.2. Effect of various processing techniques on densification (% ρ_{th}), piezoelectric strain coefficient (d_{33}) and electromechanical coupling coefficient (k_P) of the NKN/ NKN-based ceramics.

S.N.	Monolithic/ modified	Sintering temperature (T_s, °C)/ processing	% ρ_{th}	d_{33} (pC/N)	k_P (%)	Ref.
1.	Un-doped	1050 - 1325 (Conventional)	93.4 - 98.5	80 - 110	31 - 40	[132, 169, 172, 184, 185]
2.	Mg (1 mol. %) doped	1125 (Conv.)	97.1	-	45	[131]
3.	Modified with Li (4 to 7 mol. %)	1020 - 1100 (Conv.)	90.6 - 95.0	152 - 240	35 - 38	[186, 188]
4.	Modified with Li (4 mol. %) and Ta (15 mol. %)	1090 (Conv.)	98.0	206	38 - 40	[188]
5.	Modified with $LiNbO_3$ (5.8 mol. %)	1020 - 1080 (Conv.)	-	314	41.2	[187]
6.	Modified with $LiTaO_3$ (0 - 16 mol. %) and Sb (7 mol. %)	1060 - 1120 (Conv.)	-	242 - 400	36 - 54	[189]
7.	Modified with $BaTiO_3$ (5 mol. %)	1060 (Conv.)	90.0	225	36	[190]
8.	Modified with LiF (5 mol. %)	1020 (Conv.)	91.0	152	38	[148, 149]
9.	Un-doped	1080 - 1100 (Hot pressing)	99.0	160	48	[83]
10.	Modified with Li (5 mol. %)	850 - 1150 (Hot pressing)	98.8 - 99.8	-	-	[150]
11.	Un-doped	1120 (Cold isostatic pressing)	93.4	-	-	[191]
12.	Modified with Li (6 mol. %)	1075 (CIP)	94.34	123	27	[62]
13.	Modified with $BaTiO_3$ (2 mol. %)	1100 - 1250 (CIP)	98.4	104	29	[155]

14.	Modified with $LiNbO_3$ (5 to 6 mol. %)	1040 - 1100 (CIP)	-	235	44	[154]
15.	Modified with $SrTiO_3$ (5 mol. %)	1100 - 1250 (CIP)	98.4	96	32.5	[156]
16.	Modified with $LiTaO_3$ (5 mol. %)	1110 (CIP)	97.0	200	36	[153]
17.	Un-doped	1040 - 1100 (Spark plasma sintering)	98.0	-	38	[158]
18.	Un-doped	920 (SPS)	96.0 - 99.0	148	39 - 48	[152, 192, 193]
19.	Modified with $LiTaO_3$ (8 mol. %)	980 - 1000 (SPS)	98.0	185	50	[195]
20.	Modified with Li (5 mol. %) & Ta (1 mol. %)	850 - 1000 (SPS)	99.2	225 - 243	44 - 50	[196, 197, 198]
21.	Modified with Li (4 mol. %) & Ag (6 mol. %)	980 (SPS)	97.4	127	-	[194]
22.	Un-doped	800 (Hot isostatic pressing)	94	40	-	[151]
23.	Modified with LiF (5 mol. %)	1020 (Reduced atm. conv. sintering)	95.0	138	36	[148, 149]
24.	-	1090 (Sol gel - Conv. sintering)	102.66	418	54	[133]

2.4.3. Chemical modification

Apart from non-conventional sintering routes, property enhancement with chemical modification is a multifaceted and economical technique for the improvement in densification as well as piezoelectric and electrical properties of NKN-based ceramics. Malice et al. [199] investigated the effect of 0.5 atom. % doping of alkaline earth metals at A-site of NKN as $(Na_{0.5}K_{0.5})_{1-2y}$ - AE_yNbO_3 (y = .005), (AE = Ca, Sr, Ba, Mg) which was

sintered at 1115 °C for 2 h. It has been found that Ca^{2+} and Sr^{2+} doping results in the improved piezoelectric property (d_{33} up to 95 pC/N) as compared to undoped NKN (d_{33} = 80 pC/N), which is attributed to the modification in phase transition temperature [Table 2.3]. However, increased densification was only observed with Sr^{2+} from 94.4 % ρ_{th} (undoped NKN) to 96.0 % ρ_{th}. Chang et al. [200] investigated the effect of the addition of 0.5 mol. % $AETiO_3$ (AE = Ca, Sr, Mg, Ba) with $N_{0.5}K_{0.5}NbO_3$ after sintering at 1115 °C for 2 h. In perovskite structure of NKN, doping of Ca^{2+} (ionic radii = 0.135 nm), Ba^{2+} (0.160 nm), Sr^{2+} (0.144 nm) on A-site ions such as, Na^{+} (0.139 nm) and K^{+} (0.164 nm) while, an addition of Ti^{4+} (0.061 nm) on B-site Nb^{5+} (0.064 nm) ion, results in an increase in unit cell parameters of NKN. While doping of Mg^{2+} (0.072 nm) on A-site along with the addition of Ti^{4+} on B-site results in the shrinkage of its unit cell parameters and causes poor and inhomogeneous microstructure. Therefore, $MgTiO_3$ (0.5 mol. %) addition to NKN, shows poor densification (90.9 % ρ_{th}) and piezoelectric properties (d_{33} = 51 pC/N, k_P = 15 %, Q_m = 70) as compared to undoped NKN (ρ_r = 96.4 % ρ_{th}, d_{33} = 122 pC/N and k_P = 38 %, Q_m = 124). The increase in unit cell parameters contributes to the piezoelectric as well as electrical properties of NKN [Table 2.3]. Therefore, 0.5 mol. % of $CaTiO_3$, $SrTiO_3$ and $BaTiO_3$ addition to NKN exhibit good densification (95.8 - 97.8 % ρ_{th}) and relevant electrical properties (d_{33} = 85 - 116 pC/N and k_P = 26 - 39 %, Q_m = 156 - 180) [200]. A similar experiment has been performed to analyze the effect of Ca^{2+} and Ba^{2+} dopants in $N_{0.5}K_{0.5}NbO_3$ upto 2 mol. % after sintering at the temperature of 1125 °C for 2 h [201]. The maximum densification and piezoelectric properties for both Ca^{2+} or Ba^{2+} dopants were observed at 0.5 mol. % addition, above which densification reduces. It has been suggested that Ca^{2+} and Ba^{2+} ions preferably replaces to Na^{+} and K^{+}, respectively, with almost similar ionic radii. Therefore, the doping of Ca^{2+} ions,

above 0.5 mol. % reduces the densification, preferably due to the reduction of sodium phase [201]. However, the addition of Ba^{2+} at higher concentrations (> 0.5 mol. %) reduces the densification and piezoelectric properties due to the formation of a potassium-based secondary phase [201]. Zuo et al. [132] also reported that the abnormal grain growth during sintering results in reduced consolidation and piezoelectric properties. The authors suggested that the addition of CdO (1 mol. %) to NKN-based ceramics shows abnormal grain growth behavior during sintering and exhibits lower densification (ρ_r = 95.3 % ρ_{th}, T_s = 1100 °C / 4 h). However, similar densification was observed with ZnO-doped (1 mol. %) NKN-based ceramics at the lower sintering temperature (1000 °C / 4 h), which undergo controlled grain growth. [132]. Further, it has been explored that the doping of similar valence ions on A and B sites such as, Li^+ on A-site and Ta^{5+} and Sb^{5+} on B-site of ABO_3 i.e., $(Na_{0.52}K_{0.44}Li_{0.04})(Nb_{0.86}Ta_{0.10}Sb_{0.04})O_3$ textured NKN-based ceramics results in better piezoelectric properties (d_{33} = 416 pC/N, k_P = 61 %) [202]. It has been suggested that the improvement in piezoelectric properties is observed due to the modification in phase boundaries after shifting of different phase transition temperatures, as discussed in pervious section [202]. It has also been investigated that the doping of Zr^{4+} or Ti^{4+} ions (0.5 mol. %) on the Nb site of $N_{0.5}K_{0.5}NbO_3$ also results in enhancement in piezoelectric properties (d_{33} = 124 - 134 pC/N and k_P = 33 - 35 %) [203]. It happens due to the formation of oxygen vacancy defects, which restricts the domain wall motion and results in stability in the piezoelectric behavior of ceramics [203]. The influence of grain size on the piezoelectric and electrical properties of ceramics can be understood in a way that grain boundaries are amorphous in nature, which reduces overall crystallinity and consequently, the ferroelectricity. As grain size decreases, the grain boundaries increases, which weakens the ferroelectricity of the material [204].

As previously discussed in section 2.3, that the formation of MPB in the processing of NKN-based ceramics results in improvement in the piezoelectric properties. Several additives have been reported that enhances the piezoelectric properties of $N_{0.5}K_{0.5}NbO_3$ ceramics such as, 2 mol. % $BaTiO_3$ (d_{33} = 104 pC/N and k_P = 29 %), 6 mol. % $LiNbO_3$ (d_{33} = 235 pC/N and k_P = 42 %), 5 mol. % $LiTaO_3$ (d_{33} = 200 pC/N and k_P = 36 %) and 2 mol. % $SrTiO_3$ (d_{33} = 92 pC/N and k_P = 26.6 %) [153, 154, 155, 156]. It was demonstrated that the improved piezoelectric properties were attributed due to the formation MPB at the mentioned composition of additives. The effect of various dopants on the densification, piezoelectric properties, and dielectric constant are summarized in Table 2.3.

Table 2.3. Effect of doping on densification, piezoelectric (d_{33}) and dielectric (ε_r) properties of NKN.

Secondary phase	**Increase/ decrease in densification (% ρ_{th})**	**d_{33} (pC/N)**	**Electromech. Coup. Coeff. (k_p)**	**ε_r**	**Ref.**
Ca^{++} (0.5 mol. %)	94.4 to 93.8 %	95	-	495	[199]
Mg^{++} (0.5 mol. %)	94.4 to 91.2 %	-	-	-	..do..
Sr^{++} (0.5 mol. %)	94.4 to 96.0 %	95	-	500	..do..
Ba^{++} (0.5 mol. %)	94.4 to 94.1 %	-	-	-	..do..
Ca^{++} (0.5 mol. %)	96.4 to 97.8 %	116	39 %	411	[200]
Mg^{++} (0.5 mol. %)	96.4 to 90.9 %	51	15 %	480	..do..
Sr^{++} (0.5 mol. %)	96.4 to 97.1 %	110	35 %	448	..do..
Ba^{++} (0.5 mol. %)	96.4 to 95.8 %	85	26 %	393	..do..
ZnO (1 mol. %)	96.0 to 97.0 %	117	44 %	652	[132]
SnO_2 (1 mol. %)	96.0 to 98.0 %	108	39 %	627	..do..

Sc_2O_3 (1 mol. %)	96.0 to 94.2 %	100	26 %	578	..do..
CdO (1 mol. %)	96.0 to 95.3 %	107	42 %	493	..do..
$BaTiO_3$ (2 mol. %)	96.0 to 98.4 %	104	29 %	1003	[155]
$LiNbO_3$ (6 mol. %)	96.2 to 96.4 %	235	42 %	-	[154]
$LiTaO_3$ (5 mol. %)	96.0 to 97.0 %	200	36 %	570	[153]
$SrTiO_3$ (2 mol. %)	96.2 to 98.0 %	92	26.6 %	873	[156]

2.5. Piezoelectricity and biocompatibility

Several studies suggest that the polarized piezoelectric bioceramics and biopolymers improve the osteogenesis through various ways [5, 38, 55, 56, 59, 63, 64, 65]. The electrical potential, induced in piezoelectric ceramics can potentially enhance the bioactivity and cellular response for hard tissue regeneration [Fig. 2.7] [17, 39, 42, 205, 206, 207].

2.5.1. Origin of biomineralization and cytocomptibility

In vitro biomineralization study on polarized piezoelectric $BaTiO_3$ ceramic demonstrated the deposition of calcium phosphate (CaP) layer on the negatively polarized surface, while no CaP layer was observed on the positively charged surface [Fig. 2.7 (A)] [39]. Due to electrostatic interaction between Ca^{2+} ions, present in simulated body fluid (SBF) and negatively charged surface, deposition of Ca^{2+} ions takes place on the polarized surfaces [39]. The anions (HPO_4^- and OH^-), in turn, interact with these deposited Ca^{2+} ions and, form CaP layer on the negatively polarized surfaces [Fig. 2.7 (A)]. However, Cl^- ions, present in SBF are attracted towards positively charged surfaces, which do not support the formation of the CaP layer [39] [Fig. 2.7 (A)]. Similarly, it has been demonstrated that the negatively polarized surface of HA- Li modified (6 mol.%) NKN (LNKN)-HA functionally graded

material almost doubled the rate of apatite formation [right part of Fig. 2.7 (A)] as compared to non-polarized monolithic HA (briefly explained in section 2.5.4.1.) [207]. Zhau et al. [206] elucidated enhanced cell proliferation on polarized Ti - 10 vol. % polyvinylidene fluoride (PVDF) polymer [Fig. 2.7 (B)]. The cations (Ca^{2+}, H^{+} ions) from the biological fluid, adhere on the negatively charged surface. These cations further attract negatively charged proteins (like integrin, fibronectin) and cytomembrane. Consequently, the cell adhesion and proliferation on the negatively charged PVDF-Ti increase. Ca^{2+} ions, present in the apatite layer, activate cell adhesion factors [205] [Fig. 2.7 (C)]. Ca^{2+} ions, adhered on the apatite rich polarized surface, enter into the cells and move towards the nearest cell [205]. Such kind of transportation of Ca^{2+} ions between the cells promotes the cell-cell adhesion and anchoring of cells on the CaP layer, formed on the negatively polarized ceramic surfaces [205]. Similarly, negatively polarized piezoelectric ceramic enhance the cell growth as compared to their positively polarized surfaces [Fig. 2.7 (D)] [17].

As discussed above, the negatively polarized surface attracts cations like, Ca^{2+} ions present in the biological fluid, a phenomenon which serves as a stimulus for the adsorption of proteins and subsequently, promotes cellular adhesion [17, 205]. However, positively charged surface attracts anions like Cl^{-}, OH^{-}, etc, which restricts the adhesion of proteins as well as cells [17]. Apart from above mentioned *in vitro* response, *in vivo* assessment of unpolarized and polarized β-PVDF polymer samples was made by the implantation in rat's femur [42]. It has been observed that neo trabecular bone regeneration takes place on the polarized polymer samples after 4 weeks of implantation, which was almost absent in case of unpolarized polymers of identical macromolecular chemistry, for the similar period (4 weeks) of implantation [Fig. 2.7 (E)]. The mechanical stimulus, induced by physiological loadings in

rat's femur generates a voltage gradient on the polarized implant surfaces, which is responsible for the increased bone growth.

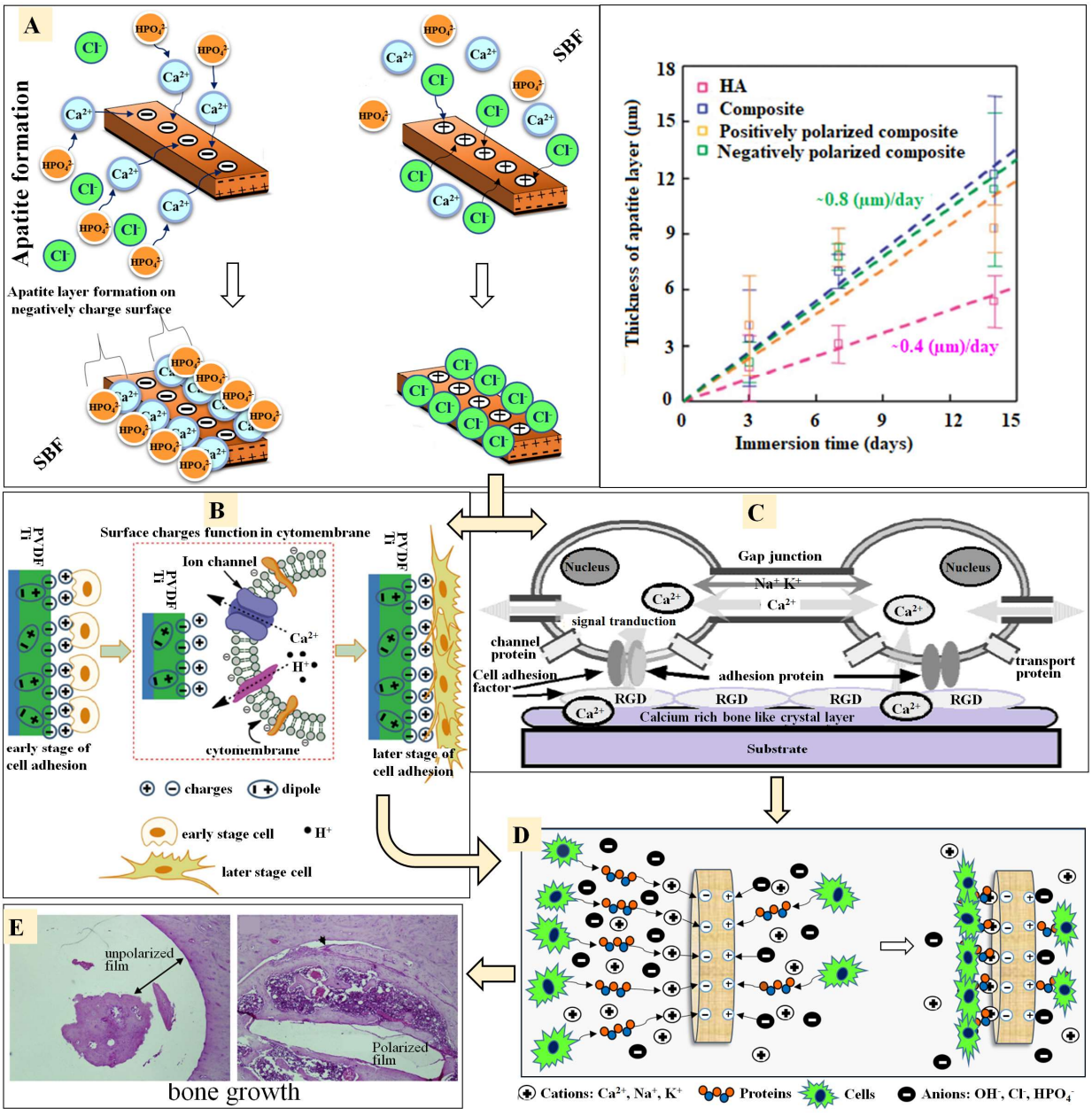

Fig. 2.7. Surface polarization induced bioactivity and cellular response, in vitro and in vitro. Polarized surfaces of piezoelectric materials promote the adsorption of apatite ions (Ca^{2+}, HPO_4^{2-}) or proteins and cell adhesion, which consequently influence the hard tissue regeneration. (A) Schematic illustrating the mechanism of accelerated apatite layer

formation on negatively charged surface as compared to the positively charged surface [39]. The polarization induced enhanced rate of apatite formation on HA-LNKN-HA functionally graded material (FGM) as compared to unpolarized FGM and HA (Reproduced with the permission from publisher, Ref. [207]). (B) Schematic representing the polarization induced enhanced osteogenesis. Cations (like Ca^{2+} ions and H^{+} ions) from the physiological environment are attracted towards the negatively charged PVDF-Ti surface. Consequently, these cations attract negatively charged cytomembrane (Reproduced with the permission from the publisher, Ref. [206]). (C) An illustration of neuroblastoma cell response on polarized HA surface. Na^{+} and Ca^{2+} work as neurotransmitters between two cells through gap junction. Ca^{2+} activates protein adhesion factors and consequently, enters into the cells through these adhesive proteins and moves towards the neighboring cell through gap junction (Reproduced with the permission from the publisher, Ref. [205]). (D) Schematic demonstration of the influence of surface polarity on the interaction between the sample surface and constituents of culture media such as cations, anions, proteins and cells [17, 205]. Negatively charged surface attracts cations, followed by proteins as well as cells. Positively charged surface attracts anions, which inhibits the protein adsorption. (E) H & E stained images, representing the healing of defects (double arrow) on the unpolarized and polarized β-PVDF film, implanted in rat's femur for 4 weeks. Unpolarized β-PVDF implanted film could not exhibit neobone formation after 4 weeks of implantation; however, the defect on the polarized β-PVDF implanted film was about to be completely covered by bone marrow like spongy tissue and trabecular bone tissue after 4 weeks of implantation (Reproduced with the permission from the publisher, Ref. [42]).

2.5.2. Origin of bone healing

The damaged tissues can be healed by the piezoelectricity induced electrical stimulation as well as direct mechanical stimulation [30, 40, 44, 208]. These mechanisms can be elaborated through two independent moduli [Fig. 2.8]. According to the first module, piezoelectric scaffolds generate electrical potentials under the influence of functional loads. Such type of electrical stimulation activates voltage-gated Ca^{2+} channels and stretch activated calcium channels pathways, which results in an increase in intracellular Ca^{2+} ions [Fig. 2.8] [40, 44]. In addition, the local electrical field can modify the configuration of membrane receptors and opens receptor channels, which allow an influx of intracellular Ca^{2+} ions from the endoplasmic reticulum [Fig. 2.8] [40, 44]. These increased Ca^{2+} ions in cells activate calcium modulated proteins as well as calcineurin (a kind of calcium dependent protein phosphatase) [30, 40]. These calcineurin proteins react with the phosphorylated nuclear factor of activated cells (NF-AT-PO_4) and convert it into dephosphorylated nuclear factors of activated cells (NF-AT) [30, 40]. These dephosphorylated NFs-AT translocate to the nucleus, where they combine with other proteins and result in gene transcription [Fig. 2.8]. Gene transcription promotes the synthesis of TGF-β and BMP-2 and consequently, regulates cell metabolism and ECM synthesis [30, 40].

According to second module, mechanical stimulation directly activates mechanoreceptors, such as integrins [30, 209]. The activated integrins translocate protein kinase C (PKC) to the cell membrane and activate MAP Kinase (MAPK) pathways for transmembrane signaling [30, 209] and consequently, transfer extracellular mechanical signals to actin [209]. RACK 1 protein (intracellular receptor) associated with integrin, binds with the PKC domain. Therefore, RACK1 mediated PKC-integrin interaction plays a key role in transmembrane

signal transduction [30, 209, 210]. Now, these signaling cascades transfer towards the nucleus and interact with mechanosensitive transcription factors and consequently, excutes gene transcription [30, 209].

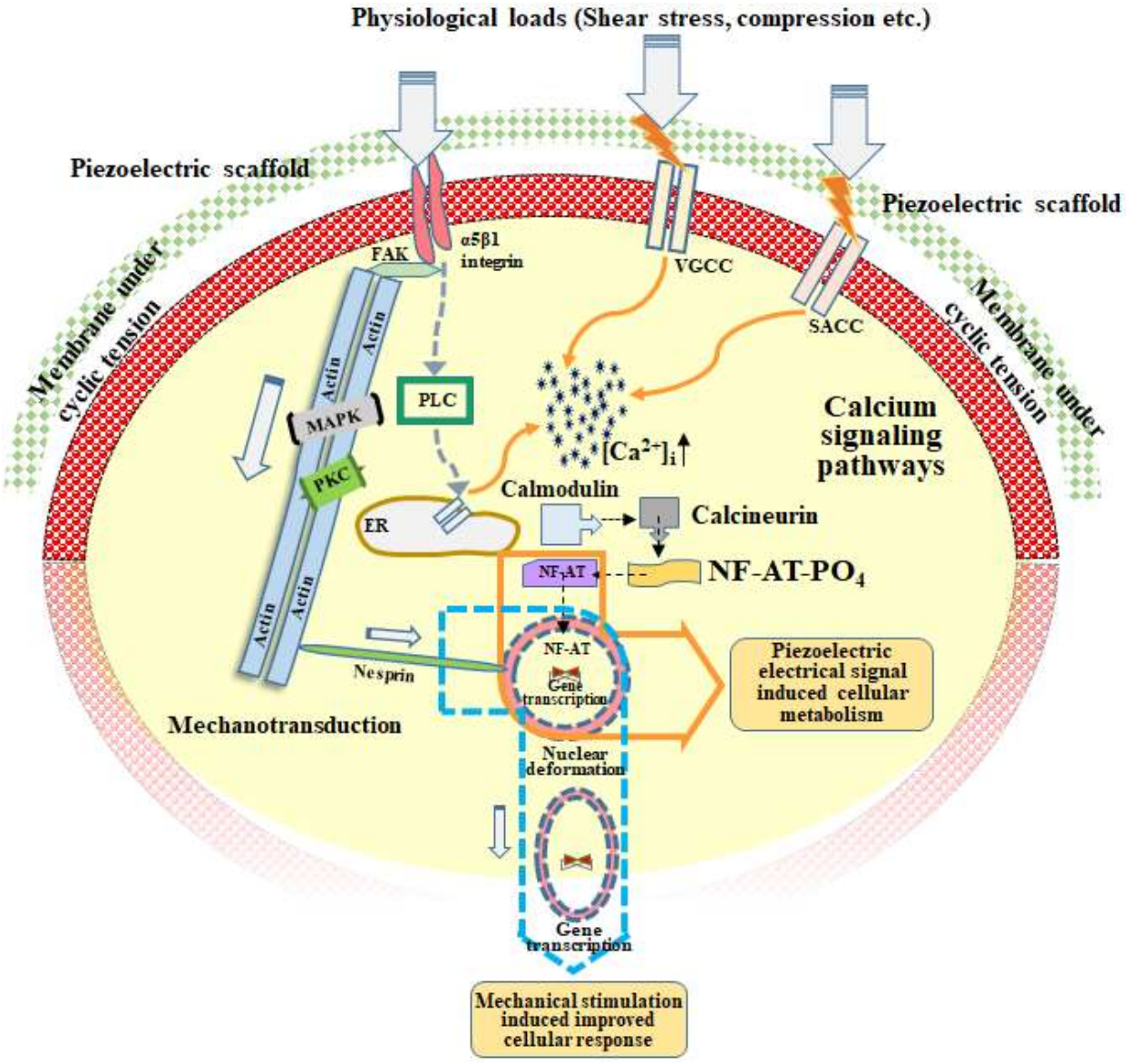

Fig. 2.8. Schematic illustration of the effect of mechanical stimulation on cell metabolism through intracellular electrical signal transduction, leading to activation of mechanoreceptors [30, 40, 44, 209]. Electromechanical signals facilitate outside-in Ca^{2+} ions influx through the opening of voltage gated Ca^{2+} channels (VGCC) and stretch activated

calcium channels (SACC) [40, 44]. Consequently, intracellular ions increase which activate the calmodulated protein and calcineurin [30, 40]. These calcium activated calcineurin dephosphorylates the phosphorylated nuclear factor of activated cells (NF-AT) and shifts towards the nucleus, where it executes gene transcription [30, 40]. Mechanically stimulated membrane receptors open up receptor channels and permit intracellular Ca^{++} ions from endoplasmic reticulum calcium stores [40, 44]. Also, physiological loads directly activate mechanoreceptors of the cell membrane like integrin, which actuate PKC (protein kinase C) and MAPK (mitogen activated protein kinase) signaling pathways [30, 209, 210]. These signaling cascade propagates towards the nucleus, where it interacts with mechanosensitive transcription factor and results in gene transcription [30, 209, 210].

The polarized (at 13 kV for 30 min.) piezoelectric $BaTiO_3$ - polymer [poly(vinylidene fluoride trifluoroethylene)] nanocomposite membranes demonstrated long lasting electrical charge storage capability. These biomaterials can facilitate the differentiation of rat bone marrow mesenchymal stem cells (BMSCs) into osteoblast cells [28]. The implantation of such polarized piezoelectric biocomposite in the calvarial site defect of rat bone has been demonstrated to promote early bone regeneration [28]. The mechanical deformation of bone collagen induces both, negative (under compression) as well as positive (under tension**)** potentials due to piezoelectricity [15]. Natural bones possess inherent negative zeta potential (- 5 mV**)** [15]. The negative charges, developed due to the compression of bone collagen, increase overall zeta potential as well as streaming potential in natural living bone [15]. This stress-stimulated electrical potential enhances the electroosmosis, and consequently, decreases the hydraulic permeability and increases the stiffness of bone [15].

2.5.3. Influence of electrical stimulation on the biological response

The application of optimal electrical stimulation results in enhanced proliferation and differentiation of human mesenchymal stem cells on biomaterials surfaces, which subsequently, assists in bone repair and regeneration [16, 17, 21, 24, 25]. The cellular response can also be enhanced by improving the conductivity of the substrate surface in a controlled manner [25]. Apart from the improved cellular response, the application of electrical field with specific pulse rate results in electroporation, which can be utilized for cancer treatment [17, 24]. Electrical stimulation can also control the directional movement of cells [25, 27]. In absence of an electric field, a cell membrane exhibits negative potential. The application of a direct current electrical field (dcEF) hyperpolarizes the anodal side membrane of the cell [25, 27]. Consequently, Ca^{2+} ions diffuse at the anodal side membrane of the cell. This increased amount of Ca^{2+} ions on the anode side results in depolymerization of actin, which causes shrinkage in cell size at the anodal end. At the same time, due to the depolarization at the cathode side membrane of the cell, the number of Ca^{2+} ions decreases, which causes the polymerization of actin and protrusion on this side of the cell. Such kind of changes in cell morphology promotes the cell movement towards the cathode side [25, 27]. However, the depolarization of the cathode side membrane of the cell opens its voltage-gated Ca^{2+} channels and consequently, increases the amount of intracellular Ca^{2+} ions [25]. Therefore, the amount of Ca^{2+} ions on both, cathodal side (due to the influx of extracellular Ca^{2+} ions) and on the anodal side (due to diffusion), causes a net movement of cells either towards cathode side or anode side, where the number of Ca^{2+} ions are less [25]. In other words, the direct current electrical field (dcEF) can control the net movement of the cells [25, 27]. Such type of controlled cell locomotion through electrically modified endogenous

charges leads to an increased attachment of cells on the wounded site that assists in wound healing. Such a phenomenon also prevents cellular accumulation on the cancerous site which is used in cancer treatment.

The efficacy of a number of piezoelectric bioceramics and biopolymers as a prospective substitute for electrically-active bone tissue is described in subsequent sections, which reveal the potentiality of piezoelectric materials as next generation materials for orthopedic implant applications.

2.5.4. Biomaterials-based perspective

2.5.4.1. NKN-based piezoelectric ceramics

Nilson et al. [55] examined the biocompatibility of NKN using human monocytes. Jalalian et al. [57] fabricated the dense ferroelectric NKN nanofibers with the help of sol-gel electro-spinning route and reported cube on cube growth of NKN nano-crystals in the crystallographic direction [001]. Such textural evolution in nanofibers suggested good potential of the electrically polarized NKN nanofibers as a scaffold for repair and regrowth of damaged / injured tissues [57]. The space charge on the polarized surfaces of NKN-based ceramics plays an important role in modulating the biological responses, such as protein adsorption, cell proliferation, etc. [56, 62, 63].

Chen et al. [56] reported that the polarized (@ 25 kV/cm) NKN increases protein adsorption on both, positively (0.43 mg-cm^{-2}) as well as negatively (0.45 mg-cm^{-2}) charged surfaces as compared to unpolarized (0.34 mg-cm^{-2}) surface. This study indicates that protein adsorption is independent of charge polarity. However, a significant increase in cell density has been reported on the negatively polarized surface than positively polarized as well as unpolarized surfaces, while cultured with MC3T3 osteoblasts cells [56]. More recently, Yao et al. [211]

investigated that polarized NKN shows significantly higher spreading and proliferation of rBMSCs cells as compared to unpolarized NKN. In another study, the addition (30 vol.%) of polarized NKN with 1393 bioglass results in comparatively higher cell proliferation than monolithic 1393 bioglass [212]. Lithium modified NKN ($Li_{.06}Na_{.5}K_{.44}NbO_3$, LNKN) ceramics possess excellent piezoelectric properties (d_{33} = 222) [213], alongwith superior biocompatibility as compared to unmodified NKN [61, 62, 63]. LNKN (polarized at ~ 22 - 24 kV/cm) exhibits excellent chemical stability and hydrophilicity against biological fluid, which indicates its suitability for orthopedic applications [61]. Electrically treated LNKN surface results in the rapid rate of apatite formation [63]. LNKN (polarized at E-field intensity of 22 - 24 kV/cm) supports 33 % higher growth of osteoblasts on the polarized surface, as compared to that on the unpolarized surface [62]. The NKN has been potentially utilized to induce the piezoelectricity in HA-NKN functionally graded material (FGM) [207, 214]. In FGM development, the piezoelectric NKN layer has been introduced between HA layers [214]. Such a concept of FGM development has been reported to increase the polarizability of HA by more than three times without affecting its excellent biocompatibility. However, the incorporation of the LNKN layer between HA layers increases the polarizability up to six times [207].

As discussed earlier, polarization plays very important role in cellular functioning. The augmented polarizability of HA can potentially increase cellular growth and proliferation. The findings of above-mentioned studies are quite appealing in terms of augmented *in vitro* biocompatibility, which is attributed to the surface charge potential of the polarized piezoelectric NKN. Therefore, the clinical implications of polarized NKN based ceramics can be realized as the physiological loads can generate surface electrical charge, which can

stimulate bone regeneration [30, 40]. Apart from the applications in bone tissue engineering, NKN-based ceramics can be utilized in nerve and skin replenishment as well as drug delivery [215].

2.5.4.2. Other piezoelectric ceramics

$BaTiO_3$ exhibits phase transformation from symmetrical cubic (paraelectric or non-polar) to an asymmetric (ferroelectric or polar) structure below its Curie temperature (130 °C), which occurs due to the relative atomic displacements between the positive centroid Ti^{4+} and face centered O^{2-} ions [5, 39]. Hwang et al. [39] performed *in vitro* bioactivity on $BaTiO_3$ ceramics, polarized above and below its Curie temperature. The Ca/ P ratio was recorded to be 1.5 - 1.7 on negatively charged $BaTiO_3$ surface, polarized above Curie temperature (i.e., 160 °C, E_p = 5 kV/cm). However, this ratio was 1.2 to 1.5 on the negatively charged surface, when polarized below Curie temperature at the same polarizing field [39]. A similar experiment has been performed by Park et al. [216] on $BaTiO_3$ ceramics, polarized above its Curie temperature (i.e., T = 160 °C, E_p = 5 kV/cm). A thick layer of CaP has been observed on the negatively charged surface of the piezoelectric sample [Fig. 2.7 (A)]. Similarly, negatively charged $BaTiO_3$ thin film has also been demonstrated to enhance the cellular functionality of L929 mouse fibroblast cells than positively charged as well as uncharged films [217]. The anticipated toxicity concern of $BaTiO_3$ particulates has been addressed by intra-articular injection of HA-40 wt.% $BaTiO_3$ particles (up to 25 mg/ml) in the knee joint of mice (Fig. 2.9) [218]. The activity and weight of mice were observed to be normal up to 7 days of post-injection. Histopathological analyses suggest that the injected particles were neither translocated to any of the major organs such as heart, kidney, liver, lung etc. nor caused any adverse effect to these organs [218]. These results confirm the absence of any

systemic toxicity of such piezo-biocomposites. It has been demonstrated that the injected particles were accumulated in the close vicinity of knee joint region without causing any inflammatory/ foreign body reaction [218].

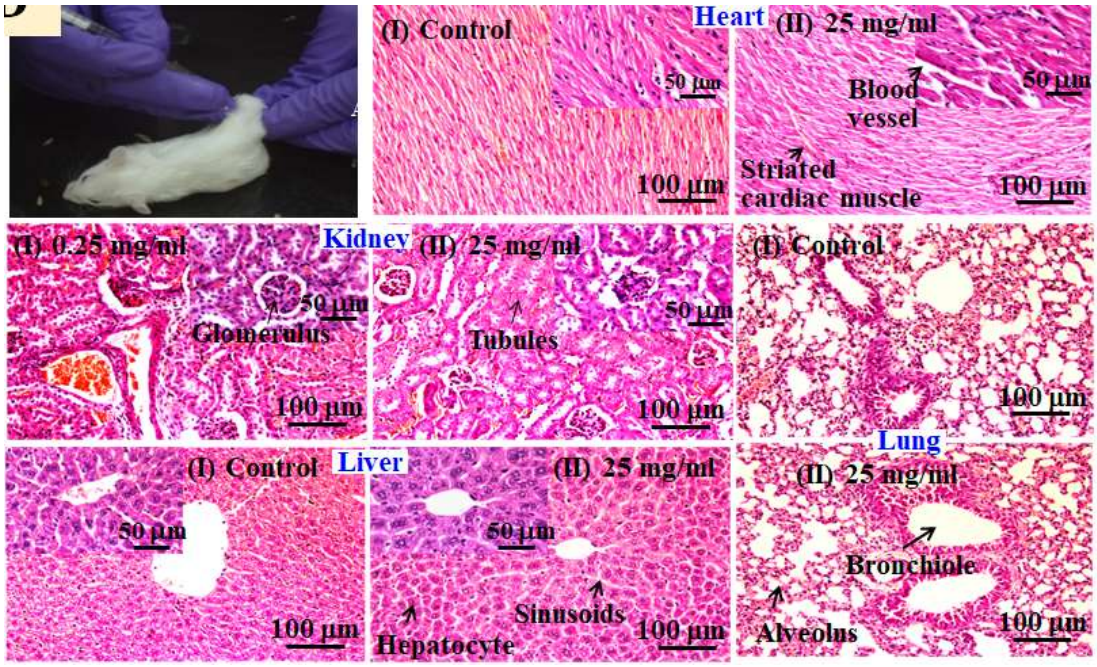

Fig. 2.9. Intra-articularly injected HA-40 wt.% $BaTiO_3$ particulate in the knee joint of mice could not cause any systematic toxicity in vital organs, such as heart, kidney, liver and lung at 7 days of post-injection, as evident from representative fluorescent images (Reproduced with the permission from the publisher, Ref. [218]).

$MgSiO_3$ (MS) possesses an asymmetric tetragonal perovskite structure, which is responsible for its piezoelectricity and spontaneous polarization [93]. The biodegradable nature of $MgSiO_3$ facilitates the piezoelectric implant to be easily replaced by newly developed bone tissue [136]. A porous scaffold consisting of HA nanowire - $MgSiO_3$ nanocomposite with Chitosan polymer i.e., HA-MS-CS [(HA-MS) : CS = 7 : 3 weight ratio] demonstrates enhanced rat BMSC [135]. Although, biodegradability facilitates cell growth and bone

regeneration with $MgSiO_3$ based scaffolds, the uncontrolled biodegradability limits their *in vivo* trials upto small animal models.

$LiNbO_3$ is a well-known ferroelectric material with excellent polarizability (spontaneous polarization, P_s = 78 μC/ cm^2) [137] at room temperature, which can be easily reversed by the application of the electric field. Apart from stable polarizability, $LiNbO_3$ also possesses good pyroelectric (P_r = 103.9 μC/m^2°K) [91] as well as piezoelectric properties (d_{33} = 23 pC/N) [65]. The electroactive $LiNbO_3$ surface adsorbs the organic molecules, like d-cysteine, which helps in stimulating polarized $LiNbO_3$ surface for protein adsorption [219]. Carville et al. [64] demonstrated that the charged surfaces of $LiNbO_3$ induces ionic exchange and protein interaction from cell media which consequently, results in significant enhancement in the proliferation of MC3T3 osteoblast cells, irrespective of charge polarity. In another study, it has been reported that the negatively charged surfaces facilitate significant cellular (NIH-3T3) elongation with more spreaded cell morphology as compared to the positively charged surfaces [137]. The negatively polarized $LiNbO_3$ surface promote the adhesion of cations, which further attracts electronegatively charged cellular membrane. However, positively charged surface attracts negatively charged ions, which restricts the adhesion of cells and in fact, causes cell migration [137]. In contrast, positively charged surface of $LiNbO_3$ exhibits 15% higher wound healing (cellular migration) capability than the negatively charged surface, which was almost double than that of the glass control surface [137]. On the other hand, Vanek et al. [65] elucidated a different hypothesis that the positively charged surface of polarized $LiNbO_3$ substrate preferably adsorbs electronegatively charged cell-adhesion proteins such as fibronectin and vitronectin. Therefore, the cell differentiation is promoted on

the positively charged surface (0.037 ALP / μg of BCA protein) as compared to the negatively charged surface (0.030 ALP / μg of BCA protein) of $LiNbO_3$ [65].

$KNbO_3$ is an emerging piezoelectric perovskite material having its application in the biomedical field as a bio-probe for disease diagnosis [69, 138, 139]. $KNbO_3$ nanowires also find their application in scanning light imaging in life sciences, due to their second harmonic generation with larger non-linear stable polarizability, at room temperature. Therefore, it has the ability to be used as a tunable coherent light source [138]. $KNbO_3$ nanocrystals, coated with amino dextrin (AD), have been demonstrated as a bio-marker for the diagnosis of non-tumor cells, as AD coated $KNbO_3$ nano-crystals suitably attach with the human lung derived BEAS-2B non-tumor cells [139]. In addition, $KNbO_3$ nanoparticles are suggested to be highly toxic for prostate cancerous cells (DU-145), which enables the application of $KNbO_3$ in prostate cancer treatment [69].

Zinc has been proved as an important element that stimulates the osteoblastic activities [220]. Owing to its piezoelectric nature, nanosized ZnO sheets develop a local electric field in the response of inherent mechanical force from the cells, which improves the metabolic activity of human SaOS-2 osteoblast-like cells and macrophages [44]. Due to the inherent stress from cells on the piezoelectric nanosheets and locally developed electrical charges, the membrane potential of adjacent cell changes. Consequently, voltage gated Ca^{2+} channels and stretch activated Ca^{2+} channels open, which allows the influx of extracellular Ca^{2+} ions [44]. There are number of literature reports which suggest that an optimized amount of ZnO reinforcement to a biomaterial causes a reasonable increase in the compatibility with fibroblasts, osteoblasts, stem cells, etc. [221, 222, 223].

Nakhmanson et al. [224] investigated the piezoelectricity and spontaneous polarization in boron nitride nanotubes (BNNT). BNNT supports the differentiation of hMSCs into osteoblast cells by releasing a trace amount of boron in culture medium and the stress applied from BNNT fibers on the hMSC cells [70]. Such kind of stress causes stretching of cells that activate actin filament and consequently, results in enhanced osteogenesis [70]. Another factor, which promotes the osteogenesis of BNNT is their positive affinity for cellular protein [225]. The adherence and proliferation of MG-63 and hMSCs are enhanced on Ackerminate - BN composite scaffold [226]. The electrospun mats, prepared by the reinforcement of 1 to 5 wt. % boron nitride on gelatin polymer, exhibit good biomineralization and cytocompatibility with HOS human osteosarcoma cells [227].

2.5.4.3. Piezoelectric polymers

The inherent piezoelectricity and biocompatibility of a specific class of polymers make them suitable for bone tissue engineering applications. These polymers can be classified as synthetic and natural piezoelectric polymers. The synthetic piezoelectric biocompatible polymers include β, γ or δ phases of polyvinylidene fluoride (PVDF) and its copolymer, poly-L-lactic acid (PLLA), polyhydroxybutyrate (PHB) and polyamides (Nylons, peptides, etc.), etc. Some of the biocompatible polysaccharides such as, cellulose (wood, ramie), chitosan, amylose (starch), and proteins such as, collagen, silk, keratin possess inherent piezoelectricity, which are categorized as natural piezoelectric polymers.

The piezoelectricity has been observed in the stretched and polarized film of PVDF polymer [228]. β, γ, and δ phases of PVDF possess permanent dipole moment and exhibit piezoelectricity [103]. The biocompatibility of piezoelectric PVDF polymeric substrates has been investigated with MC3T3-E1 osteoblast cells [29, 229, 230, 231, 232], human

mesenchymal stem cells (hMSCs) [233, 234], human adipose stem cells (hASC) [235, 236], and goat marrow stem cells [237]. Poly (L-Lactic) acid or PLLA is another synthetic polymer with reasonable piezoelectricity (d_{14} = -10 pC/N) and biodegradability [123, 238]. Barroca et al. [239] demonstrated the surface polarization induced fibronectin adsorption on PLLA film, prepared by spin coating. PLLA is currently being used to make fastening devices for orthopedic application such as bone plate, screws, pins, washers etc. due to its excellent ossiointegration [240, 241]. The piezoelectric poly 3-hydroxybutyrate or PHB (d_{14} = 1.3 pC/N) is a member of a polyester polyhydroxyalkanoates (PHA), which has been demonstrated to be biodegradable [242, 243, 244]. Several studies have been performed with PHB and its copolymers such as, PHBHV or poly (3-hydroxybutyrate-co-3-hydroxyvalerate) and PHBHH or poly-(hydroxybutyrate-co-hydroxyhexanoate)-based polymers to investigate their biocompatibility, *in vitro* [73, 245, 246, 247, 248, 249, 250].

Collagen is a natural protein, found in living bone and due to its non-centrosymmetric structure, bone exhibits piezoelectricity [6, 251]. Collagen has been proved as an excellent biocompatible material due to its reasonable cell binding ability and low antigenicity [78, 252]. In addition, the collagen-based scaffold has been reported to support the functionality of SaOS-2 osteoblast-like cells [253]. However, high degradation rate and low stiffness of natural polymers put the concern on their mechanical strength [252, 254]. Chitosan is another piezoelectric natural polysaccharide polymer, as reviewed by Martino et al. [75]. It has been demonstrated that chitosan-based polymer scaffolds exhibit several favorable characteristics to be used as orthopedic implant such as, osteoconductivity, porosity, easy molding ability, antibacterial response and minimum foreign body reaction [75]. Cellulose is another piezoelectric polysaccharide natural polymer, which can be a suitable candidate for bone

tissue applications due to its superior biocompatibility and good mechanical strength. Zaborowska et al. [77] observed that cellulose-based microporous scaffold results in significantly higher proliferation of MC3T3-E1 osteoblast cells as compared to the nanoporous scaffold.

2.6. Surface charge polarization induced antibacterial response

2.6.1. Bacterial infection

As far as the issues associated with the development of prosthetic implants are concerned, bacterial infection is among the critical issues which lead to implant failure [255, 256, 257]. The gram positive cocci (*Streptococci, Staphylococcus aureus*, *coagulase-negative staphylococci*) and gram negative bacteria (*Pseudomonas aerugenosa, Escherichia Coli* etc.) are the common bacteria associated with the infection in the prosthetic orthopedic implants [258, 259]. In general, bacteria reach the implant surface through the blood vessels route and contain a capsule of extracellular matrix (ECM) protein around them which helps in colonizing bacteria and subsequently, form a three dimensional bacterial biofilm on the implant surface [260, 261, 262]. This biofilm protects bacteria from the immune defense system and antibiotics [263, 264, 265]. Sometimes, the antibodies or immune cells, produced by the immune defense system to neutralize biofilm antigens, fail to penetrate the bacterial biofilm [266, 267, 268]. For this purpose, antibiotics have been recognized to be a suitable alternative. However, the bacteria develop resistance against antibiotics in a dose and time dependent manner [268]. Therefore, antibiotics do not remain effective for a longer duration.

2.6.2. Influence of surface charge and other external stimuli on bacteria

Gram negative bacteria consists of two layers, a thin layer of peptidoglycan (~ 5 - 10 nm), surrounded by an outer layer of lipopolysaccharides. However, gram positive bacterial cell

wall contains a single thick layer of peptidoglycan (~ 20 - 80 nm) [269, 270, 271, 272]. Although, both the bacterial cells are negatively charged, the *E. coli* bacteria possess about 1.5 times higher negative charge than that of gram positive bacteria [273, 274]. Due to specific electrical surface potentials, bacteria respond against electric or magnetic field which generates reactive oxygen species (ROS) that damage bacterial cell wall and consequently, kills the bacteria [275, 276, 277, 278, 279]. It has been reported that the magnetic field (100 mT for 4 h) inhibits the growth of *E. coli* and *S. epidermidis* bacterial cells [275, 276, 277]. In addition, the exposure of external electric field (direct current ~ 100 mA or direct current electric field ~ 1 V/cm) hinders the growth of biofilm on the implant and consequently, enhances the antibacterial response [278, 279]. Bacteria interact with polarized piezoelectric substrates by means of microelectric field of charged surfaces and electrical potential of bacterial membranes [211, 280, 281, 282]. Recently, Verma et al. [212, 283, 284] reported the surface charge induced antibacterial response of polarized piezoelectric biocomposites. Tan et al. [280] and Yao et al. [211] manipulated the electrostatic interaction by polarizing (25 kV/cm for 30 min) sodium potassium niobate ($Na_{0.5}K_{0.5}NbO_3$) piezoceramic surfaces against negatively charged membranes of *S. aureus* bacterial cells. Since, bacterial cell membrane exhibits electrical charge, it interacts with polarized surfaces. The microelectric field generates on the polarized surfaces, enhances the rate of electrolysis of water that causes breakage of hydrogen bond and consequently, produces ROS such as H_2O_2, O_2^- etc [211, 281, 285, 286]. Such ROS are toxic for the bacterial cells [211, 280, 281, 287]. Swain et al. [282] demonstrated that the polarization (4.5 kV/cm) of barium titanate – hydroxyapatite piezo-biocomposite surfaces increase the zone of inhibition (> 2 times) for *S. aureus*, *E. coli* and *P. aerugenosa* bacteria as compared to non-polarized composite surfaces.

Apart from the positively polarized surfaces, negatively polarized surfaces have also been suggested to reduce bacterial adhesion due to electrostatic repulsion between mutually opposite charged surfaces of substrate and bacteria [281, 287]. In addition, the negatively polarized surface shows excellent hydrophilicity, which reduces the bacterial cell population [17, 288, 289, 290, 291]. Singh et al. [281] reported that the viability of *E. coli* and *S. aureus* bacterial cells are reduced by 53% and 40 %, respectively on negatively charged surfaces of HA - 7.5 % ZnO bioceramic composite. External electrical or magnetic stimulation needs sophisticated device installation near the patient and tool insertion in the human body to reach to the infected implant surface during treatment which may cause additional concerns. Therefore, surface electrical treatment or surface polarization can be regarded as a suitable technique to induce the antibacterial property in prosthetic implants, prior to implantation.

Recently, it has been demonstrated that the addition of the $Na_{0.5}K_{0.5}NbO_3$ (30 vol. %) phase in HA and bioglasses (45S5 and 1393) enhances the antibacterial response of biocomposites where the inhibition of bacterial strains is observed to depend on surface charge polarity [212, 283, 284]. Apart from surface charge polarization, the presence of sodium and potassium (individual or in combination) in bacterial extracellular matrices creates an unfavorable environment for the growth of bacteria and consequently, enhances the antibacterial response [292, 293]. The antibacterial performance of any material system depends on the number of factors such as surface charge, surface chemistry, oxidative stress etc. [292, 293, 294, 295].

The piezoelectricity has been demonstrated as an intrinsic functional property to regulate the bone metabolism. In a continuous surge towards bone mimicking materials, the development of piezoelectric bioceramics and biopolymers has been discussed herein for bone tissue

engineering applications. Towards this end, number of processing related challenges, such as, densification, volatilization of alkali elements for a range of compositionally tuned piezoelectric bioceramics, in particular reference to sodium potassium niobate, have been discussed. Importantly, the piezoelectricity / electrical stimulation induced augmented bioactivity, cellular response, tissue regeneration, etc. have been highlighted with a specific emphasis on the biocompatibility of polarized piezoelectric bioceramics and biopolymers. Different ways to overcome bacterial infection on implants such as antibiotics, external stimuli (electrical and magnetic field) and surface charge polarization have been comprehensively analyzed along with their limitations. In addition, recent progress on demonstrating the efficacy of the surface charge polarization induced antibacterial response of bioceramics was also discussed.

Despite various available literatures demonstrate the potentiality of piezoelectric ceramics, however, actual mechanisms of electrical stimulation induced improved biological response of piezoelectric biomaterials are still unclear. The combined effect of electrostatic and dynamic electrical stimulation have not been explored well, as such stimuli positively affect the cellular or antibacterial response individually. Further, the effect of surface polarization on the surface characteristics such as, surface chemistry or wettability should be investigated, as such surface properties directly influence the cellular and bacterial response. The leaching behavior of biomaterials is another important factor that may affect their performance. It has been hypothesized that the external electrical stimulation influences the voltage-gated signaling pathways and thereby, improve the osteogenic response however, the actual quantitative study have not been performed yet.

By considering the above backdrops, the present study reveals the influence of the combined action of electrostatic surface polarization charge and dynamic pulsed electrical stimulation alongwith compositional modification towards improving the osteogenic response of emerging piezo-bioceramics, sodium potassium niobate [$Na_xK_{1-x}NbO_3$ (x = 0.2 - 0.8), NKN] prepared by cold isostatic pressing (Pressure: 330 MPa). Thereafter, the synergistic effect of surface polarization and compositional variation of Na and K contents in biocompatible $Na_xK_{1-x}NbO_3$ (x = 0.2 to 0.8) was investigated in improving their antibacterial performance. An *in vivo* study to examine the local and systemic toxicity of NKN nanoparticulates in rat's model has also been performed.

References

[1] E. Fukada, I Yasuda, On the piezoelectric effect of bone, J. Phys. Soci. Japan 12 (1957) 1158-1162.

[2] M. A. E. Messiery, G. W. Hastings, S. Rakowski, Ferro-electricity of dry cortical bone, J. Biomed. Eng. 1 (1979) 63-65.

[3] S. B. Lang, Pyroelectricity: occurrence in biological materials and possible physiological implications, Ferroelec. 34 (1981) 3-9.

[4] C. S. McDowell, Implanted bone stimulator and prosthesis system and method of enhancing bone growth, U.S Patent 6143035A (2000).

[5] F. R. Baxter, C. R. Bowen, I. G. Turner, A. C. E. Dent, Electrically active bioceramics: A review of interfacial responses, Annal. Biomed. Eng. 38 (2010) 2079-2092.

[6] G. W. Hastings, F. A. Mahmud, Electrical effects in bone, J. Biomed. Eng. 10 (1988) 515-521.

[7] C. Halperin, S. Mutchnik, A. Agronin, M. Molotskii, P. Urenski, M. Salai, G. Rosenman, Piezoelectric effect in human bones studied in nanometer scale, Nan. Lett. 4 (2004) 1253-1256.

[8] S. B. Lang, Pyroelectric effect in bone and tendon, Nature 212 (1966) 704-705.

[9] C. D. McCaig, M. Zhao, Physiological electrical fields modify cell behavior, BioEssays 19 (1997) 819-826.

[10] I. Yasuda, Electrical callus and callus formation by electret, Clin. Ortho. Rel. Res. 124 (1977) 53-56.

[11] C. A. L. Bassett, R. O. Becker, Generation of electric potentials by bone in response to mechanical stress, Science 137 (1962) 1063-1064.

[12] B. M. Isaacson, R. D. Bloebaum, Bone bioelectricity: What have we learned in the past 160 years?, J. Biomed. Mat. Res. 95A (2010) 1270-1279.

[13] A. G. Robling, C. H. Turner, Mechanical Signaling for Bone Modeling and Remodeling, Crit. Rev. Eukaryot. Gene Expr. 19 (2009) 319-338.

[14] Z. B. Friedenberg, C. T. Brighton, Bioelectric potentials in bone. J. Bone Joint Surg. Am. 48 (1966) 915-923.

[15] A. C. Ahn, A. J. Grodzinsky, Relevance of collagen piezoelectricity to "Wolff's Law": A critical review, Med. Eng. Phys. 31 (2009) 733-741.

[16] A. K. Dubey, S. D. Gupta, B. Basu, Optimization of electrical stimulation parameters for enhanced cell proliferation on biomaterial surfaces, J. Biomed. Mater. Res. 98B (2011) 18-29.

[17] A. K. Dubey, B. Basu, Pulsed Electrical Stimulation and Surface Charge Induced Cell Growth on Multistage Spark Plasma Sintered Hydroxyapatite Barium Titanate Piezobiocomposite, J. Am. Ceram. Soc. 97 (2014) 481-489.

[18] G. Thrivikraman, G. Madras, B. Basu, Intermittent electrical stimuli for guidance of human mesenchymal stem cell lineage commitment towards neural-like cells on electroconductive substrates, Biomaterials 35 (2014) 6219-6235.

[19] G. Thrivikraman, P. Lee, R. Hess, V. Haenchen, B. Basu, D. Scharnweber, Interplay of substrate conductivity, cellular microenvironment and pulsatile electrical stimulation towards osteogenesis of human mesenchymal stem cells *in vitro*, ACS Appi. Mat. Interf. 7 (2015) 23015-23028.

[20] K. Ravikumar, G. P. Kar, S. Bose, B. Basu, Synergistic effect of polymorphism, substrate conductivity and electric field stimulation towards muscle cell growth *in vitro*, RSC Adv. 6 (2016) 10837-10845.

[21] K. Ravikumar, S. K. Boda, B. Basu, Synergy of substrate conductivity and intermittent electrical stimulation towards osteogenic differentiation of human mesenchymal stem cells, Bioelectrochem. 116 (2017) 52-64.

[22] S. Naskar, V. Kumaran, B. Basu, Reprogramming the stem cell behaviour by shear stress and electric field modulation: Lab-on-a-chip based applications in regenerative medicine, Reg. Eng. Transl. Med. (2018) 1-29.

[23] G. Thrivikraman, S. K. Boda, B. Basu, Unravelling the mechanistic effects of electric field stimulation towards directing stem cell fate and function: a tissue engineering perspective, Biomaterials 150 (2018) 60-86.

[24] K. Ravikumar, V. Kumaran, B. Basu, Biophysical implications of Maxwell stress in electric field stimulated cellular microenvironment on biomaterial substrates, Biomaterials 209 (2019) 54-66.

[25] M. E. Mycielska, M. B. A. Djamgoz, Cellular mechanisms of direct-current electric field effects: galvanotaxis and metastatic disease, J. Cell Sci. 117 (2009) 1631-1639.

[26] A. K. Dubey, A. Mukhopadhyay, B. Basu, Interdisciplinary Engineering Sciences: Concepts and Applications, CRC Press (Taylor and Francis Group, UK) ISBN: 978-0-3673-3393-5 (2020) 358.

[27] A. H. Rajabi, M. Jaffe, T. L. Arinzeh, Piezoelectric materials for tissue regeneration: A review, Acta Biomater. 24 (2015) 12-23.

[28] X. Zhang, C. Zhang, Y. Lin, P. Hu, Y. Shen, K. Wang, S. Meng, Y. Chai, X. Dai, X. Liu, Y. Liu, X. Mo, C. Cao, S. Li, X. Deng, L. Chen, Nanocomposite membranes enhance bone regeneration through restoring physiological electric microenvironment, ACS Nano. 10 (2016) 7279-7286.

[29] C. Ribeiro, V. Sencadas, D. M. Correia, S. Lanceros-Mendez, Piezoelectric polymers as biomaterials for tissue engineering applications, Colloids and Surface B: Biointer. 136 (2015) 46-55.

[30] J. Jacob, N. More, K. Kalia, G. Kapusetti, Piezoelectric smart biomaterials for bone and cartilage tissue engineering, Inflam. Regen. 38 (2018).

[31] B. Tandon, J. Blaker, S. Cartmell, Piezoelectric materials as stimulatory biomedical materials and scaffolds for bone repair, Acta Biomater. 73 (2018) 1-20.

[32] B. Basu, Biomaterials Science and Tissue Engineering: Principles and Methods, Cambridge University Press, First edition ISBN: 9781108415156 (2017) 716.

[33] T. Eriksson, K. Nelsson, A.-K. Johansson, K. Ljjungstrom, K. Lashgari, A. Pohl, G. Westin, Synthesis of Sodium potassium niobate by sol gel, Patent No. US 8,246,929 B2 (2012).

[34] S. R. Platt, S. Farritor, K. Garvin, H. Haider, The use of piezoelectric ceramics for electric power generation within orthopedic implants, IEEE Trans. Mechatron. 10 (2005) 455-461.

[35] Chorsi, M. T., Curry, E. J., Chorsi, H. T., Das, R., Baroody, J., Purohit, P. K., Ilies, H., Nguyen, T. D., Piezoelectric Biomaterials for Sensors and Actuators, Adv. Mater. 31 (2019) 1802084.

[36] A. Sultana, S. K. Ghosh, V. Sencadas, T. Zheng, M. H. Higgins, T. R. Middya, D. Mandal, Human Skin Interactive Self-powered Wearable Piezoelectric Bio-e-skin by Electrospun Poly-L-lactic Acid Nanofibers for Non-invasive Physiological Signal Monitoring, J. Mater. Chem. B**.** J. Mater. Chem. B 5 (2017) 7352-7359.

[37] J. H. McElhaney, The charge distribution on the human femur due to load, J. Bone Joint Surg. Am. 49 (1967) 1561-1571.

[38] J. B. Park, A. F. von Recum, G. H. Kenner, B. J. Kelly, W. W. Coffeen, M. F. Grether, Piezoelectric ceramic implants: a feasibility study, J. Biomed. Mater. Res. 14 (1980) 269-277.

[39] K. S. Hwang, J. E. Song, H. S. Yang, Y. J. Park, J. L. Ong, H. R. Rawls, Effect of poling conditions on growth of calcium phosphate crystal in ferroelectric BaTiO3 ceramics, J. Mater. Sci. Mater. Medic. 13 (2002) 133-138.

[40] N. More, G. Kapusetti, Piezoelectric material - A promising approach for bone and cartilage regeneration, Med. Hypo. 108 (2017) 10-16.

[41] A. Marino, J. Rosson, E. Gonzalez, L. Jones, S. Rogers, E. Fukada, Quasi static charge interactions in bone, J. Electrostatics. 21 (1988) 347-360.

[42] C. Ribeiro, D. M. Correia, I. Rodrigues, L. Guardão, S. Guimarães, R. Soares, S. Lanceros-Méndez, In-vivo demonstration of the suitability of piezoelectric stimuli for bone reparation, Mater. Lett. 209 (2017) 118-121.

[43] K. Kapat, Q. T. H. Shubhra, M. Zhou, S. Leeuwenburgh, Piezoelectric Nano-Biomaterials for Biomedicine and Tissue Regeneration, Adv. Funct. Mater. (2020) 1909045.

[44] G. Murillo, A. Blanquer, C. Vargas-Estevez, L. Barrios, E. Ibáñez, C. Nogues, J. Esteve, Electromechanical Nanogenerator-Cell Interaction Modulates Cell Activity, Adv. Mater. 29 (2017) 1605048.

[45] Y. Liu, X. Zhang, C. Cao, Y. Zhang, J. Wei, Y. Li, W. Liang, Z. Hu, J. Zhang, Y. Wei, X. Deng, Adv. Funct. Mater. 27 (2017) 1703771.

[46] T. Zigman, S. Davila, I. Dobric, T. Antoljak, G. Augustin, D. Rajacic, T. Kovac, T. Ehrenfreund, Intraoperative measurement of bone electrical potential: a piece in the puzzle of understanding fracture healing, Injury 44 (2013) S16-S19.

[47] B. Dutta, E. Kar, N. Bose, S. Mukherjee, NiO@SiO2/PVDF: A Flexible Polymer Nanocomposite for High Performance Human Body Motion Based Energy Harvester and Tactile e-skin Mechanosensor, ACS Sustain. Chem. Eng. 6 (2018) 10505-10516.

[48] H. He, Y. Fu, W. Zang, Q. Wang, L. Xing, Y. Zhang, X. Xue, A flexible self-powered T-ZnO/PVDF/fabric electronic-skin with multi-functions of tactile-perception, atmosphere detection and self-clean, Nano Energy 31 (2017) 37-48.

[49] T. Huang, S. Yang, P. He, J. Sun, S. Zhang, D. Li, Y. Meng, J. Zhou, H. Tang, J. Liang, G. Ding, X. Xie, Phase-Separation-Induced PVDF/Graphene Coating on Fabrics toward Flexible Piezoelectric Sensors, ACS Applied Materials & Interfaces 10 (2018) 30732-30740.

[50] A. Wang, Z. Liu, M. Hu, C. Wang, X. Zhang, B. Shi, Y. Fan, Y. Cui, Z. Li, K. Ren, Piezoelectric nanofibrous scaffolds as *in vivo* energy harvesters for modifying fibroblast alignment and proliferation in wound healing, Nano Energy 43 (2018) 63-71.

[51] J. F. Li, K. Wang, F. Y. Zhu, L. Q. Cheng, F. Z. Yao, (K,Na)NbO_3-based lead-free piezoceramics: Fundamental aspects, processing technologies, and remaining challenges, J. Am. Ceram. Soc. 96 (2013) 3677-3696.

[52] B. Jaffe, W. R. Cook, and H. Jaffe, Piezoelectric Ceramics (Academic Press Limited, London, 1971).

[53] j. Tellier, B. Malic, B. Dkhil, D. Jenko, J. Cilensek, M. Kosec, Crystal structure and phase transitions of sodium potassium niobate perovskites, Solid State Sci. 11 (2009) 320-324.

[54] S. Pradhan, G. S. Roy, Study the Crystal Structure and Phase Transition of $BaTiO_3$ - A Pervoskite, Resear. 5 (2013) 63-67.

[55] K. Nelsson, J. Lidman, K. Ljjungstrom, C. Kjellman, Biocompatible material for implants, Patent No. US 6526984 B1 (2003).

[56] W. Chen, Z. Yu, J. Pang, P. Yu, G. Tan, C. Ning, Fabrication of biocompatible potassium sodium niobate piezoelectric ceramic as an electroactive implant, Materials (Basel) 10 (2017) 18-21.

[57] A. Jalalian, A. M. Grishin, Biocompatible ferroelectric (Na, K)NbO_3, Appl. Phys. Lett. 100 (2012) 012904.

[58] J. B. Park, B. J. Kelly, G. H. Kenner, A. F. von Recum, M. F. Grether, W. W. Coffeen, Piezoelectric ceramic implants: *In vivo* results, J. Biomed. Mater. Res. 15 (1981) 103-110.

[59] G. Ciofani, L. Ricotti, V. Mattoli, Preparation, characterization and *in vitro* testing of poly (lactic-co-glycolic) acid/barium titanate nanoparticle composites for enhanced cellular proliferation, Biomed. Microdev. 13 (2011) 255-266.

[60] A. K. Dubey, B. Basu, K. Balani, R. Guo, A. S. Bhalla, Multifunctionality of perovskites BaTiO3 and CaTiO3 in a composite with hydroxyapatite as orthopaedic implant materials, Integ. Ferroelect. 131 (2011) 119-126.

[61] Q. Wang, X. Chen, J. Zhu, B. W. Darvell, Z. Chen, Porous Li-Na-K niobate bone-substitute ceramics: Microstructure and piezoelectric properties, Mater. Let. 62 (2008) 3506-3508.

[62] Q. Wang, J. Yang, W. Zhang, R. Khoie, Y. Li, J. Zhu, Z. Chen, Manufacture and Cytotoxicity of a Lead-free Piezoelectric Ceramic as a Bone Substitute Consolidation of Porous Lithium Sodium Potassium Niobate by Cold Isostatic Pressing, Int. J. Oral Sci. 1 (2009) 99-104.

[63] A. K. Dubey, H. Y. Yamada, K. Kakimoto, Space charge polarization induced augmented *in vitro* bioactivity of piezoelectric (Na,K) NbO_3, J. Appl. Phys. 114 (2013) 124701.

[64] N. C. Carville, L. Collins, M. Manzo, K. Gallo, B. I. Lukasz, K. K. McKayed, J. C. Simpson, B. J. Rodriguez, Biocompatibility of ferroelectric lithium niobate and the influence of polarization charge on osteoblast proliferation and function, J. Biomed. Mater. Res. Part A 103A (2015) 2540-2548.

[65] P. Vanek, Z. Kolska, T. Luxbacher, J. A. L. García, M. Lehocky, M. Vandrovcova, L. Bacakovaand J, Petzelt, Electrical activity of ferroelectric biomaterials and its effects on the adhesion, growth and enzymatic activity of human osteoblast-like cells, J. Phys. D: Appl. Phys. 49 (2016) 175403.

[66] Z. Wu, T. Tang, H. Guo, S. Tang, Y. Niu, J. Zhang, W. Zhang, R. Ma, J. Su, C. Liu, J. Wei, *In vitro* degradability, bioactivity and cell responses to mesoporous magnesium silicate for the induction of bone regeneration, Elsevier: Coll. Sur. B: Biointer. 120 (2014) 38-46.

[67] Z. Wu, K. Zheng, J. Zhang, T. Tang, H. Guo, A. R. Boccaccini, J. Wei, Effects of magnesium silicate on mechanical property, biocompatibility, bioactivity, degradability,

osteogenesis of poly(butylene succinate) - based composite scaffolds for bone repair, J. Mater. Chem. B (RSC) 4 (2016) 7974-7988.

[68] Y. G. Kang, J. Wei, J. W. Shin, Y. R. Wu, J. Su, Y. S. Park, J. W. Shin, Enhanced biocompatibility and osteogenic potential of mesoporous magnesium silicate/polycaprolactone/wheat protein composite scaffolds, Int. J. Nanomed. 13 (2018) 1107-1117.

[69] J. G. Fisher, U. T. Thuan, M. U. Farooq, G. Chandrasekaran, Y. D. Jung, E. C. Hwang, J-J Lee, V-K Lakshmanan, Prostate Cancer Cell-Specific Cytotoxicity of Sub-Micron Potassium Niobate Powder, J. Nanosci. Nanotech. 18 (2018) 3141-3147.

[70] X. Li, W. Xiupeng, X. Jiang, M. Yamaguchi, A. Ito, Y. Bando, D. Golberg, Boron nitride nanotube-enhanced osteogenic differentiation of mesenchymal stem cells, J. Biomed. Mater. Res. Part B, Appl. biomater. 104 (2015) 323-329.

[71] C. Khatua, S. Bodhak, B. Kundu, V. K. Balla, *In vitro* bioactivity and bone mineralization of bismuth ferrite reinforced bioactive glass composites, Materialia 4 (2018) 361-366.

[72] G. Narayanan, E. Kuyinu, Poly (Lactic Acid)-Based Biomaterials for Orthopaedic Regenerative Engineering, Adv. Drug Deli. Rev. 107 (2016) 247-276.

[73] C. Mota, S. Y. Wang, D. Puppi, M. Gazzarri, C. Migone, F. Chiellini, G. Q. Chen, E. Chiellini, Additive manufacturing of poly[(*R*)-3-hydroxybutyrate-*co*-(*R*)-3-hydroxyhexanoate] scaffolds for engineered bone development, J. Tiss. Eng. Regen. Med. 11: (2017) 175-186.

[74] A. H. Abdalla, S. H. Abdel, A. K. Khalil, Fabrication of durable high performance hybrid nanofiber scaffolds for bone tissue regeneration using a novel, simple in situ

deposition approach of polyvinylalcohol on electrospun nylon 6 nanofibers, Mater. Let. 147 (2015) 25-28.

[75] D. A. martino, M. Sittinger, M. V. Risbud, Chitosan: A versatile biopolymer for orthopaedic tissue-engineering, Biomater. 26 (2005) 5983-5990.

[76] I. Amaral, A. L. Cordeiro, P. Sampaio, M. Barbosa, Attachment, spreading and short-term proliferation of human osteoblastic cells cultured on chitosan films with different degrees of acetylation, J. Biomater. Sci. Poly. ed. 18 (2007) 469-485.

[77] M. Zaborowska, A. Bodin, H. Backdahl, J. Popp, A. Goldstein, P. Gatenholm, Microporous bacterial cellulose as a potential scaffold for bone regeneration, Acta Biomater. 6 (2010) 2540-2547.

[78] C. H. Lee, A. Singla, Y. Lee, Biomedical applications of collagen, Int. J. Pharm. 221 (2001) 1-22.

[79] M. H. Shamos, L. S. Lavine, Physical bases for bioelectric effects in mineralized tissues, Clin. Orthopaed. 35 (1964) 177-188.

[80] S. Singh, S. Saha, Electrical properties of bone: A review. Clin. Orthoped. Rel. Res. 186 (1984) 249-271.

[81] M. Minary-Jolandan, M. F. Yu, Shear piezoelectricity in bone at the nanoscale, Appl. Phys. Lett. 97 (2010) 153127.

[82] G. W. Hastings, MA ElMessiery, S. Rakowsk, Mechano-electric properties of bone, Biomaterials 2 (1981) 225-233.

[83] R. E. Jaeger, L. Egerton, Hot pressing of potassium sodium Niobates, J. Am. Ceram. Soc. 45 (1962) 209-213.

[84] K. Kakimoto, Y. Hayakawa, I. Kagomiya, Low-Temperature Sintering of Dense (Na,K)NbO3 Piezoelectric Ceramics Using the Citrate Precursor Technique, J. Am. Ceram. Soc. 93 (2010) 2423-2426.

[85] D. Berlincourt, H. Jaffe, Elastic and Piezoelectric Coefficients of Single-Crystal Barium Titanate, Phys. Rev. 111(1958) 143-148.

[86] H. B. Sharma, A. Mansingh, Sol-gel processed barium titanate ceramics and thin films, Journal of material science 33 (1998) 4455-4459.

[87] T. Kimura, Q. Dong, S. Yin, T. Hashimoto, A. Sasaki, T. Sato, Synthesis and piezoelectric properties of Li-doped $BaTiO_3$ by a solvothermal approach, J. Euro. Ceram. Soc. 33 (2013) 1009-1015.

[88] D. Xue, Y. Zhou, H. Bao, C. Zhou, J. Gao, Elastic, piezoelectric, and dielectric properties of $Ba(Zr_{0.2}Ti_{0.8})O_3$-$50(Ba_{0.7}Ca_{0.3})TiO_3$ Pb-free ceramic at the morphotropic phase boundary, J. Appl. Phys. 109 (2011) 054110.

[89] S. B. Lang, Pyroelectricity: From Ancient Curiosity to Modern Imaging Tool, Phys. Tod. 58 (2005) 31-36.

[90] C. Chen, J. Ji, X. Jaio, H. Ding, Fabrication and Properties of Lithium Sodium Potassium Niobate Lead-Free Piezoelectric Ceramics, J. Adv. Microsc. Res. 12 (2017) 85-88.

[91] J. Parravicini, J. Safioui, V. Degiorgio, P. Minzioni, M. Chauvet, All-optical technique to measure the pyroelectric coefficient in electro-optic crystals, J. Appl. Phys. 109 (2011) 033106-033106.

[92] S. C. Bhatt, B. S. Semwal, Dielectric and ultrasonic properties of $LiNbO_3$ ceramics, Sol. Stat. Ion. 23 (1987) 77-80.

[93] E. Nakamachi, Y. Okuda, S. Kumazawa, Y. Uetsuji, K. Tsuchiya, H. Nakayasu, Development of Fabrication Technique of Bio-Compatible Piezoelectric Material $MgSiO_3$ by Using Helicon Wave Plasma Sputter, Trans. Jpn. Soc. Mech. Eng. Ser. A 72 (2006) 353-358.

[94] H. Nagata, K. Matsumoto, T. Hirosue, Y. Hiruma, T. Takenaka, Fabrication and Electrical Properties of Potassium Niobate Ferroelectric Ceramics, Jpn. J. Appl. Phys. 46 10 B (2007) 7084-7088.

[95] H. Birol, D. Damjanovic, N. Setter, Preparation and Characterization of $KNbO_3$ Ceramics, J. Am. Ceram. Soc. 88 (2005) 1754-1759.

[96] J. A. Bur, Measurements of dynamic piezoelectric properties of bone as a function of temperature and humidity, J. Biomech. 9 (1976) 495-507.

[97] M. Chaari, Structural and Dielectric Properties of Sintering Zinc Oxide Bulk Ceramic, Mater. Sci. Applic. 2 (2011) 764-769.

[98] D. F. Crisler, J. J. Cupal A. R. Moore, Dielectric, piezoelectric, and electromechanical coupling constants of zinc oxide crystals, Proc. IEEE 56 (1968) 225-226.

[99] M. Gupta, N. Sinha, B. Singh, N. Singh, K. Kumar, B. Kumar, Piezoelectric, Dielectric, Optical and Electrical Characterization of Solution Grown Flower-Like ZnO Nanocrystal, Mater. Lett. 63 (2009) 1910-1913.

[100] K. Kim, A. Hsu, X. Jia, S. Kim, Y. Shi, M. Dresselhaus, T. Palacios, J. Kong, Synthesis and Characterization of Hexagonal Boron Nitride Film as a Dielectric Layer for Graphene Devices, ACS nano. 6 (2012) 8583-8590.

[101] C. Ban, L. Li, L. Wei, Electrical properties of O-self-doped boron-nitride nanotubes and the piezoelectric effects of their freestanding network film, RSC Adv. 8 (2018) 29141-29146.

[102] P. Martins, J. Nunes, G. Hungerford, D. Miranda, A. Ferreira, V. Sencadas, S. L. Mendez, Local variation of the dielectric properties of poly(vinylidene fluoride) during the α- to β-phase transformation, Phys. Lett. A - Phys. Lett. A. 373 (2009) 177-180.

[103] P. Martins, A. C. Lopes, S. Lanceros-Mendez, Electroactive phases of poly(vinylidene fluoride): determination, processing and applications, Prog. Polym. Sci. 39 (2014) 683-706.

[104] J. Gomes, J. Nunes, V. Sencadas, S. L. Mendez, Influence of the β-phase content and degree of crystallinity on the piezo- and ferroelectric properties of poly(vinylidene fluoride), Smart Mater. Struc. 19 (2010) 065010.

[105] J. Song, G. Zhao, B. Li, J. Wang, Design optimization of PVDF-based piezoelectric energy harvesters, Heliyon. 3 (2017) e00377.

[106] R. Al-Jishi, P. Taylor, Equilibrium polarization and piezoelectric and pyroelectric coefficients in poly(vinylidene fluoride), J. Appl. Phys. 57 (1985) 902-905.

[107] H. Ohigshi, Electromechanical properties of polarized polyvinylidene fluoride films as studied by the piezoelectric resonance method, J. Appl. Phys. 47 (1976) 949-955.

[108] G. W. Day, C. A. Hamilton, R. L. Peterson, Jr. R. J. Phelan, L. O. Mullen, Effects of poling conditions on responsivity and uniformity of polarization of PVF2 pyroelectric detectors, Appl. Phys. Lett. 24 (1974) 456-458.

[109] H. Xu, Dielectric properties and ferroelectric behavior of poly(vinylidene fluoride-trifluoroethylene) 50/50 copolymer ultrathin films, J. Appl. Polym. Sci. 80 (2001) 2259-2266.

[110] K. Omote, H. Ohigashi, K. Koga, Temperature dependence of elastic, dielectric, and piezoelectric properties of 'single crystalline' films of vinylidene fluoride trifluoroethylene copolymer, J. Appl. Phys. 81 (1997) 2760-2769.

[111] N. Meng, R. Mao, W. Tu, X. Zhu, R. Wilson, E. Bilotti, M. Reece, Processing and characterization of free standing highly oriented ferroelectric polymer films with remarkably low coercive field and high remnant polarization, Polymer. 100 (2016) 69-76.

[112] K. Koga, H. Ohigashi, Piezoelectricity and related properties of vinylidene fluoride and trifluoroethylene copolymers, J. Appl. Phys. (ISSN 0021-8979) 59 (1986) 2142-2150

[113] T. Furukawa, Piezoelectricity and pyroelectricity in polymers, *IEEE Trans. Elec. Insu.* 24 (1989) 375-394.

[114] S. Hikosaka, H. Ishikawa, O. Yoshimichi, Effects of Crystallinity on Dielectric Properties of Poly (L-lactide). IEEJ Trans. Fund. Mater. 129 (2009) 217-222.

[115] T. Ochiai, E. Fukada, Electromechanical properties of Poly-L-Lactic Acid, Jpn. J. Appl. Phys. 37 (1998) 3374-3376.

[116] J. Malmonge, L. F. Malmonge, G. C. Fuzari Jr, S. M. Malmonge, W. K. Sakamoto, Piezo and dielectric properties of PHB-PZT composite, Pol. Comp. 30 (2009) 1333-1337.

[117] E. Fukada, Y. Ando, Piezoelectric properties of poly-β-hydroxybutyrate and copolymers of β hydroxybutyrate and β-hydroxyvalerate, Int. J. Bio. Macro. 8 (1986) 361-366.

[118] A. J. Lovinger, Recent Developments in the Structure, Properties, and Applications of Ferroelectric Polymers, 1985 Jpn. J. Appl. Phys. 24, 18-22

[119] L. F. Brown, J. I. Scheinbeim, B. A. Newman, High frequency dielectric and electromechanical properties of ferroelectric nylon 11, Ferroelec. 171 (1995) 321-327.

[120] J. Lee, Y. Takase, B. Newman, J. Scheinbeim, Effect of Annealing on the Ferroelectric Behavior of Nylon 7 and Nylon 11, J. Pol. Sci. B Pol. Phys. 29 (1991) 279-286.

[121] J. W. Lee, Y. Takase, B. A. Newman, J. I. Scheinbeim, Ferroelectric polarization switching in nylon-11, J. Pol. Sci. B Pol. Phys. 29 (1991) 273-277.

[122] C. G. A. Lima, R. S. Oliveira, S. D. Figueiro, C. Wehmann, J. Goes, S. Sombra, DC conductivity and dielectric permittivity of collagen-chitosan films, Mater. Chem. Phys. 99 (2006) 284-288.

[123] E. Fukada, Piezoelectricity of biopolymers, Biorh. 32 (1995) 593-609.

[124] S. K. Ghosh, D. Mandal, High-Performance Bio-Piezoelectric Nanogenerator Made with Fish Scale, Appl. Phys. Lett. 109 (2016) 103701.

[125] A. M. D. G. Plepis, D. K. D. Gupta, Dielectric and pyroelectric characterization of anionic and native collagen, Polym. Eng. Sci. 36 (1996) 2932-2938.

[126] P. Thakur, N. Hoque, S. Roy, P. Biswas, S. Das, P. Ray, Md. Saikh, B. Bagchi, Bio-Waste Crab Shell extracted Chitin Nanofiber Based Superior Piezoelectric Nanogenerator, J. Mater. Chem. A 6 (2018) 13848-13858.

[127] H. Athenstaedt, Pyroelectric behaviour of integument structures and of thermo-, photo- and mechanoreceptors, Anat. Embryo. 136 (1972) 249-271.

[128] T. Putzeys, M. Wübbenhorst, Polarization Domain Information on Insect Wing Chitin using the Scanning PyroElectric Microscope (SPEM), IEEE Trans. Dielec. Elec. Insul. 22 (2015) 1394-1400.

[129] R. E. Newnham, Properties of materials, Book Oxford university press, ISBN 0-19-852075-1 (hbk) ISBN 0-19-852076-x (pbk) (2005) 176.

[130] K. C. Kao, dielectric phenomenon in solids, Book Elsevier Acad. Press ISBN: 0-12-396561-6 (2004) 215.

[131] M. Kosec, D. Kolar, On activated sintering and electrical properties of $NaKNbO_3$, Mat. Res. Bull. 10 (1975) 335-340.

[132] R. Zuo, J. Rodel, R. Chen, L. Li, Sintering and electrical properties of lead free $Na_{.5}K_{.5}NbO_3$ piezoelectric ceramics, J. Am. Ceram. Soc. 89 (2006) 2010-2015.

[133] H. Wang, R. Zuo, J. Fu, Y. Liu, Sol-gel derived (Li, Ta, Sb) modified sodium potassium niobate ceramics: Processing and piezoelectric properties, J. alloy. Comp. 509 (2011) 936-941.

[134] V. Raghvan, Materials science and engineering, Prentice Hall, India, fifth edition, ISBN-81-203-2455-2 (2004) 420-421.

[135] T. W. Sun, W. L. Yu, Y. J. Zhu, R. L. Yang, Y. Q. Shen, D. Y. Chen, Y. H. He, F. Chen, Hydroxyapatite Nanowire @ Magnesium Silicate Core−Shell Hierarchical Nanocomposite: Synthesis and Application in Bone Regeneration, ACS Appl. Mater. Inter. 9 (2017) 16435-16447.

[136] S. Feng, J. Li, X. Jiang, X. Li Y. Pan, L. Zhao, A. Boccaccini, K. Zheng, L. Yang, J. wei, Influences of mesoporous magnesium silicate on hydrophilicity, degradability, mineralization and primary cells response to wheat protein based biocomposite, J. Mater. Chem. B 4 (2016) 6428-6436.

[137] M. Valentina, G. Oriella, M. Laura, G. Simonetta, F. Pietro, Effects of Lithium Niobate Polarization on Cell Adhesion and Morphology, ACS Appl. Mater. Inter. 7 (2015) 18113-18119.

[138] Y. Nakayama, P. J. Pauzauskie, A. Radenovic, R. M. Onorato, R. J. Saykally, J. Liphardt, P. Yang, Tunable nanowire nonlinear optical probe, Nature 447 (2007) 1098-1101.

[139] R. Ladj, T. Magouroux, M. Eissa, M. Dubled, Y. Mugnier, R. L. Dantec, C. Galez, J. P. Valour, H. Fessi, A. Elaissari, Aminodextran-coated potassium niobate ($KNbO_3$) nanocrystals for second harmonic bio-imaging, Colloids and Surfaces A: Physicochem. Eng. Aspects 439 (2013) 131-137.

[140] M. D. Maeder, D. Damjanovic, Lead Free Ferroelectric Materials, Piezo. Mater. Dev. Edited: N. Setter. Lausanne, Switzerland, (2002) 389-412.

[141] H. Y. Park, C. W. Ahn, H. C. Song, J. H. Lee, S. Nahm, K. Uchino, H. G. Lee, Microstructure and piezoelectric properties of $0.95(Na_{0.5}K_{0.5})NbO_3$-$0.05BaTiO_3$ ceramics, Appl. Phys. Lett. 89 (2006) 062906.

[142] M. Kosec, B. Malic, A. Bencan, T. Rojas, KNN-based piezoelectric ceramics. In: A. Safari, E. Akdogan, Piezoelectric and acoustic materials for transducer applications, Springer Sci. Bus. Med., New York (2008) 81-102.

[143] B. Malic, J. Bernard, A. Bencan, M. Kosec, Influence of zirconia addition on the microstructure of $K_{0.5}Na_{0.5}NbO_3$ ceramics, J. Eur. Ceram. Soc. 28 (2008) 1191-1196.

[144] H. Y. Park, I. T. Seo, J, H. Choi, S. Nahm, H. G. Lee, Low-temperature sintering and piezoelectric properties of $(Na_{0.5}K_{0.5})NbO_3$ lead-free ceramics, J. Am. Ceram. Soc. 93 (2010) 36-39.

[145] I. T. Seo, H. Y. Park, N. V. Dong, M. K. Choi, S. Nahm, H. G. Lee, B. H. Choi, Microstructure and piezoelectric properties of $(Na_{0.5}K_{0.5})NbO_3$ lead-free piezoelectric ceramics with V_2O_5 addition, IEEE Trans. Ultrason. Ferro. Freq. Cont. 56 (2009) 2337-2342.

[146] J. Bernard, A. Bencan, T. Rojac, J. Holc, B. MaliC, M. Kosec, Low-temperature sintering of $K_{0.5}Na_{0.5}NbO_3$ ceramics, J. Am. Ceram. Soc. 91 (2008) 2409-2411.

[147] M. S. Kim, S. J. Jeong, J. S. Song, Microstructure and piezoelectric properties in the Li_2O-Excess $0.95(Na_{0.5}K_{0.5})NbO_3$-$0.05LiTaO_3$ Ceramics, J. Am. Ceram. Soc. 90 (2007) 3338-3340.

[148] K. Kobayashi, Y. Doshida, Y. Mizuno, C. A. Randall, A Route forwards to narrow the performance gap between PZT and lead-free piezoelectric ceramic with low oxygen partial pressure processed $(Na_{0.5}K_{0.5})NbO_3$, J. Am. Ceram. Soc. 95 (2012) 2928-2933.

[149] K. Kobayashi, C. A. Randall, M. Ryu, Y. Doshida, Y. Mizuno, New opportunity in alkali niobate ceramics processed in low oxygen partial pressure, In *Proc. of 2012 21st IEEE International Symposium on Applications of Ferroelectrics Held Jointly with 11th IEEE Eur. Conf. Applic. of Pol. Dielec. IEEE, ISAF/ECAPD/PFM 2012* 6297768 (2012).

[150] G. H. Haertling, Properties of Hot-Pressed Ferroelectric Alkali Niobate Ceramics, J. Am. Ceram. Soc. - Dis. Not. 50 (1967).

[151] H. Maiwa, Dielectric and electromechanical properties of (K, Na)NbO_3 ceramics prepared by Hot isostatic pressing, Ferroelec. 491 (2016) 71-78.

[152] B. Zhang, J. Li, K. Wang, H. Zhang, Compositional Dependence of Piezoelectric Properties in $Na_xK_{1-x}NbO_3$ Lead-Free Ceramics Prepared by Spark Plasma Sintering, J. Am. Ceram. Soc. 89 (2006) 1605-1609.

[153] Y. Guo, K. Kakimoto, H. Ohsato, (Na0.5K0.5)NbO_3-$LiTaO_3$ lead-free piezoelectric ceramics, Mater. Lett. 59 (2005) 241-244.

[154] Y. Guo, K. Kakimoto, H. Ohsato, Phase transitional behavior and piezoelectric properties of (Na0.5K0.5)NbO_3-$LiNbO_3$ ceramics,Appl. Phys. Lett. 85 (2004) 4121-4123.

[155] Y. Guo, K. Kakimoto, H. Ohsato, Structure and Electrical Properties of Lead-Free $(Na_{0.5}K_{0.5})NbO_3$-$BaTiO_3$ Ceramics, Jpn. J. appl. Phys. 43 (2004) 6662-6666.

[156] Y. Guo, K. Kakimoto, H. Ohsato, Dielectric and piezoelectric properties of lead-free $(Na_{0.5}K_{0.5})NbO_3$-$SrTiO_3$ ceramics, Solid state commun. 129 (2004) 279-284.

[157] V. J. Tennery, K. W. Hang, Thermal and X-Ray diffraction studies of $NaNbO_3$-$KNbO_3$ system, J. Appl. Phys. 39 (1968) 4749-4753.

[158] R. Wang, R. Xie, T. Sekiya, Y. Shimojo, Y. Akimune, N. Hirosaki, M. Itoh, Piezoelectric properties of spark plasma sintered $(Na_{.5}K_{.5})NbO_3$-$PbTiO_3$ ceramics, Jpn. J. Appl. Phys. 41 (2002) 7119-7122.

[159] Barbara Malic, J. Koruza, J. Hrescak, J. Bernard, K. Wang, J. G. Fisher, A. Bencan, Sintering of Lead-Free Piezoelectric Sodium Potassium Niobate Ceramics, Materials 8 (2015) 8117-8146.

[160] Y. J. Dai, X. W. Zhang, G. Y. Zhou, Phase transitional behavior in $K_{0.5}Na_{0.5}NbO_3$-$LiTaO_3$ ceramics, Appl. Phys. Lett. 90 (2007) 262903.

[161] S. J. Zhang, R. Xia, T. R. Shrout, G. Zang, J. Wang, Piezoelectric properties in provskite $0.948(K_{0.5}Na_{0.5})NbO_3$-$0.052LiSbO_3$ lead-free ceramics, J. Appl. Phys. 100 (2006) 104108.

[162] S. Zhang, R. Xia, H. Hao, H. Liu, T. R. Shrout, Mitigation of thermal and fatigue behavior in$K_{0.5}Na_{0.5}NbO_3$-based lead free piezoceramics, Appl. Phys. Lett. 92 (2008) 152904.

[163] J. Rodel, K. G. Webber, R. Dittmer, W. Jo, M. Kimura, D. Damjanovic, Transferring lead-free piezoelectric ceramics into application, J. Eur. Ceram. Soc. 35 (2015) 1659-1681.

[164] E. Hollenstein, D. Damjanovic, N. Setter, Temperature stability of the piezoelectric properties of Li-modified KNN ceramics, J. Eur. Ceram. Soc. 27 (2007) 4093-4097.

[165] J. Wu, D. Xiao, J. Zhu, Potassium-Sodium Niobate Lead-Free Piezoelectric Materials: Past, Present, and Future of Phase Boundaries, Chem. Rev. 115 (2015) 2559-2595.

[166] S. J. Zhang, R. Xia, T. R. Shrout, Modified $(K_{0.5}Na_{0.5})NbO_3$ based lead-free piezoelectrics with broad temperature usage range, Appl. Phys. Lett. 91 (2007) 132913.

[167] E. K. Akdogan, K. Kerman, M. Abazari, A. Safari, Origin of high piezoelectric activity in ferroelectric $(K_{0.44}Na_{0.52}Li_{0.04})(Nb_{0.84}Ta_{0.1}\ Sb_{0.06})O_3$ ceramics, Appl. Phys. Lett. 92 (2008) 112908.

[168] B. Malic, A. Benan, T. Rojac, M. Kosec, Lead-free Piezoelectrics Based on Alkaline Niobates: Synthesis, Sintering and Microstructure, Acta Chim. Slov. 55 (2008) 719-726.

[169] L. Egerton and D. M. Dillon, Piezoelectric and Dielectric Properties of ceramics in the System Potassium-Sodium Niobate, J. Am. Ceram. Soc. 42 (1959) 438-442.

[170] Z. S. Ahn, W. A. Schulze, Conventionally Sintered $(Na_{0.5}\ K_{0.5})NbO_3$ with Barium Additions, J. Am. Ceram. Soc. 70 (1987) 18-21.

[171] R. Wang, R. Xie, T. Sekiya, Y. Shimojo, Fabrication and characterization of potassium-sodium niobate piezoelectric ceramics by spark-plasma-sintering method, Mater. Res. Bull. 39 (2004) 1709-1715.

[172] D. Jenko, A. Bencan, B. Malič, J. Holc, and M. Kosec, Electron microscopy Studies of Potassium-Sodium Niobate Ceramics, Microscop. Microanal. 11 (2005) 572-580.

[173] H. Du, Z. Li, F. Tang, S. Qu, Z. Pei, W. Zhou, Preparation and piezoelectric properties of $(K_{0.5}Na_{0.5})NbO_3$ lead-free piezoelectric ceramics with pressure-less sintering, Mater. Sci. Eng. 131 (2006) 83-87.

[174] E. Ringgaard, T. Wurlitzer, Lead-free piezoceramics based on alkali niobates, J Eur. Ceram. Soc. 25 (2005) 2701-2706.

[175] J. Koruza, B. Malic, M. Kosec, Microstructure evolution during sintering of sodium niobate, J. Am. Ceram. Soc. 94 (2011) 4174-4178.

[176] J. Acker, H. Kungl, M. J. Hoffmann, Influence of alkaline and niobium excess on sintering and microstructure of sodium-potassium Niobate $(K_{0.5}Na_{0.5})NbO_3$. J. Am. Ceram. Soc. 93 (2010) 1270-1281.

[177] A. Popovic, L. Bencze, J. Koruza, B. Malic, Vapor pressure and mixing thermodynamic properties of the $KNbO_3$-$NaNbO_3$ system, RSC Adv. 5 (2015) 76249-76256.

[178] F. Madaro, R. Saeterli, J. R. Tolchard, M. A. Einarsrud, R. Holmestad, T. Grande, Molten salt synthesis of $K_4Nb_6O_{17}$, $K_2Nb_4O_{11}$ and KNb_3O_8 crystals with needle- or plate-like morphology, Cryst. Eng. Comm. 13 (2011) 1304-1313.

[179] R. German, P. Suri, S. Park, Review: Liquid phase sintering, J. Mater. Sci. 44 (2009) 1-39.

[180] M. Matsubara, T. Yamaguchi, K. Kikuta, S. Hirano, Sintering and piezoelectric properties of potassium sodium niobate ceramics with newly developed sintering aid, Jpn. J. Appl. Phys. 44 (2005) 258-263.

[181] S. H. Park, C. W. Ahn, S. Nahm, J. S. Song, Microstructure and piezoelectric properties of ZnO-added $(Na_{0.5}K_{0.5})NbO_3$ ceramics, Jpn. J. Appl. Phys. 43 (2004) L1072-L1074.

[182] J. Ryu, J. J. Choi, B. D. Hahn, D. S. Park, W. H. Yoon, K. Y. Kim, Sintering and piezoelectric properties of KNN ceramics doped with KZT, IEEE Trans. Ultrason. Ferroelectr. Freq. Control 54 (2007) 2510-2515.

[183] K. Chen, F. Zhang, J. Zhou, X. Zhang, C. Li, L. An, Effect of borax addition on sintering and electrical properties of $(K_{0.5}Na_{0.5})NbO_3$ lead-free piezoceramics, Ceram. Int. 41 (2015) 10232-10236.

[184] H. Birol, D. Damjanovic, and N. Setter, Preparation and Characterization of $(K_{0.5}Na_{0.5})$ NbO_3 Ceramic, J. Eur. Ceram. Soc., 26, 861-866 (2006).

[185] M. Feizpour, T. Ebadzadeh, D. Jenko, solid-state sintering of $(K_{0.5}Na_{0.5})NbO_3$ synthesized from an alkali-carbonate-based low temperature calcined powder, MTAEC9 49 (2015) 975-982.

[186] H. C. Song, K. H. Cho, H. W. Park, C. W. Ahn, S. Nahm, K. Uchino, H. G. Lee, Microstructure and piezoelectric properties of $(1-x)(Na_{0.5}K_{0.5})NbO_3$-$xLiNbO_3$ ceramics, J. Am. Ceram. Soc. 90 (2007) 1812-1816.

[187] P. Zhao, B. Zhang, J. Li, High piezoelectric d_{33} coefficient in Li-modified lead-free $(Na,K)NbO_3$ ceramics sintered at optimal temperature, Appl. Phys. Lett. 90 (2007) 242909.

[188] Y. Zhen, J. Li, Normal sintering of $(K,Na)NbO_3$-based ceramics: Influence of sintering temperature on densification, microstructure, and electrical properties, J. Am. Ceram. Soc. 89 (2006) 3669-3675.

[189] R. Zuo, W. J. Fu, D. Lv, Phase Transformation and Tunable Piezoelectric Properties of Lead-Free $(Na_{0.52}K_{0.48-x}Li_x)(Nb_{1-x-y}Sb_yTa_x)O_3$ System, J. Am. Ceram. Soc. 92 (2009) 283-285

[190] C. W. Ahn, H. Y. Park, S. Nahm, K. Uchino, H. G. Lee, H. J. Lee, Structural variation and piezoelectric properties of $0.95(Na_{0.5}K_{0.5})NbO_3$-$_{0.05}BaTiO_3$ ceramics, Sensors and Actuators A 136 (2007) 255-260.

[191] J. Hrescak , A. Bencan , T. Rojac , B. Malic, The influence of different niobium pentoxide precursors on the solid-state synthesis of potassium sodium niobate, J. Eur. Ceram. Soc. 33 (2013) 3065-3075.

[192] M. Bah, F. Giovannelli, F. Schoenstein, G. Feuillard, E. Le Clezio, I. Monot-Laffez, High electromechanical performance with spark plasma sintering of undoped $K_{0.5}Na_{0.5}NbO_3$ ceramics, Ceram. Inter. 40 (2014) 7473-7480.

[193] M. Bah, F. Giovannelli, F. Schoenstein, C. Brosseau, J. Deschamps, F. Dorvaux, L. Haumesser, E. Le Clezio, Isabelle Monot-Laffez, Ultrasonic transducers based on undoped lead-free $(K_{0.5}Na_{0.5})NbO_3$ Ceramics, Ultrason. 63 (2015) 23-30.

[194] M. Li, N. Y. Chan, D. Wang, Improved thermal stability of the piezoelectric properties of (Li, Ag)-co-modified (K, Na) NbO3-based ceramics prepared by spark plasma sintering, J. Am. Ceram. Soc. 100 (2017) 2984-2990.

[195] J. Abe, M. Kobune, K. Kitada T. Yazawa, Effects of Spark-Plasma Sintering on the Piezoelectric Properties of High-Density $(1-x)(Na_{0.5}K_{0.5})NbO_3$-$xLiTaO_3$ Ceramics, J. Kor. Phys. Soc. 51 (2007) 810-814

[196] Z. Shen, J. Li, K. Wang, S. Xu, Electrical and Mechanical Properties of Fine-Grained Li/Ta-Modified (Na,K)NbO3-Based Piezoceramics Prepared by Spark Plasma Sintering, J. Am. Ceram. Soc. 93 (2010) 1378-1383.

[197] Y. Zhena, J. Li , K. Wang, Y. Yan, L. Yu, Spark plasma sintering of Li/Ta-modified (K,Na)NbO3 lead-free piezoelectric ceramics: Post-annealing temperature effect on phase structure, electrical properties and grain growth behavior, Mater. Sci. Eng. B 176 (2011) 1110-1114.

[198] R. J. Lopez, F. G. Gonzalez, J. M. Zarate, R. G. Escalona, S. D. L. T. Diaz, M. E. V. Castrejon, Piezoelectric properties of Li-Ta co-doped potassium-sodium niobate ceramics prepared by spark plasma and conventional sintering, J. alloy. Comp. 509 (2011) 3837-3842.

[199] B. Malic, J. Bernard, J. Holc, D. Jenko, M. Kosec, Alkaline-Earth Doping in (K,Na)NbO_3 Based Piezoceramics, J. Eur. Ceram. Soc. 25 (2005) 2707-2711.

[200] Y. Chang, Z. Yang, L. Wei, B. Liu, Effects of $AETiO_3$ Additions on Phase Structure, Microstructure and Electrical Properties of $(K_{0.5}Na_{0.5})NbO_3$, Mater. Sci. Eng. A 437 (2006) 301-305.

[201] J. Taub, L. Ramajo, M. Castro, M. Miriam, Phase structure and piezoelectric properties of Ca- and Ba-doped K1/2Na1/2NbO_3 lead-free ceramics, Ceram. Inter. 39 (2013) 3555–3561.

[202] Y. Saito, H. Takao, T. Tani, T. Nonoyama, K. Takatori, T. Homma, T. Nagaya, M. Nakamura, Lead free piezoceramics, Nature, 432 (2004) 84-87.

[203] X. Vendrell, J. E. García, X. Bril, D. A. Ochoa, L. Mestres, G. Dezanneau, Improving the functional properties of $(K_{0.5}Na_{0.5})NbO_3$ piezoceramics by acceptor doping, J. Eur. Ceram. Soc. 35 (2015) 125-130.

[204] A. S. Shaikh, R. W. Vest, and G. M. Vest, Dielectric properties of ultrafined grained $BaTiO_3$, IEEE Trans. Ultrason. Ferroelec. Freq. Cont. 36 (1989) 407-412.

[205] M. Ohgaki, T. Kizuki, M. Katsura, K. Yamashita, Manipulation of selective cell adhesion and growth by surface charges of electrically polarized hydroxyapatite, Journal of Biomedical Materials Research Part A. 57 (2001) 366-373.

[206] Z. Zhou, W. Li, T. He, L. Qian, G. Tan C. Ning, Polarization of an electroactive functional film on titanium for inducing osteogenic differentiation, Sci. rep. 6 (2016) 35512.

[207] A. K. Dubey, R. Kinoshita K. Kakimoto, Piezoelectric sodium potassium niobate mediated improved polarization and *in vitro* bioactivity of hydroxyapatite, RSC Adv. 5 (2015) 19638-19646.

[208] F. Martino, A. R. Perestrelo, V. Vinarsky, S. Pagliari, G. Forte, Cellular Mechanotransduction: From Tension to Function, Front Physiol. 9 (2018) 824.

[209] H. S. Lee, S. J. M. Sadler, M. O. Wright, G. Nuki, R. A. Jamal, D. M. Salter, Activation of Integrin-RACK1/PKCα signalling in human articular chondrocyte mechanotransduction, Osteoarth. Cartil. 10 (2002) 890-897.

[210] D. M. Rosen, H. Khaner, J. Lopez, Identification of intracellular receptor proteins for activated protein kinase C, Proc. Natl. Acad. Sci. of the USA 88 (1991) 3997-4000.

[211] T. Yao, J. Chen, Z. Wanga, J. Zhai, Y. Li, J. Xing, S. Hu, G. Tan, S. Qi, Y. Chang, P. Yu, C. Ning, The antibacterial effect of potassium-sodium niobate ceramics based on controlling piezoelectric properties, Coll. Sur. B: Biointer. 175 (2019) 463-468.

[212] A. S. Verma, D. Kumar, A. K. Dubey, Antibacterial and cellular response of piezoelectric Na0.5K0.5NbO3modified 1393 bioactive glass, Mat. Sci. Eng.: C 116 (2020) 111138.

[213] Q. Chen, D. Lan, Y. Chen, Z. Xu, X. Yue, D. Xiao, J. Zhu, Influence of Sintering Temperatures on the Properties of Lithium Sodium Potassium Niobate Piezoelectric Ceramics, Mater. Res. Soc. Symp. Proc. 888 (2005) 11.1-11.6.

[214] A. K. Dubey, K. Kakimoto, A. Obata and T. Kasuga, Enhanced polarization of hydroxyapatite using the design concept of functionally graded materials with sodium potassium niobate, RSC Adv. 4 (2014) 24601-24611.

[215] L. Atanasoska, R. Radhakrishnan, S. Schewe, Medical devices employing piezoelectric materials for delivery of therapeutic agents. In: Google patents; (2014) US8702682B2.

[216] Y. J. Park, K. S. Hwanga, J. E. Song, J. L. Ong, H. R. Rawls, Growth of calcium phosphate on poling treated ferroelectric $BaTiO_3$ ceramics, Biomaterials 23 (2002) 3859-3864.

[217] I. J. Jeong, H. I. Kwak, J. L. Kim, H. R. Ong, Rawls, Y. J. Park, The 81st General Session of the Intern. Assoc. Dent. Res., Goteberg, Sweden, (2003).

[218] A. K. Dubey, G. Thrivikraman, B. Basu, Absence of systemic toxicity in mouse model towards $BaTiO_3$ nanoparticulate based eluate treatment, J. Mat. Sci. Mater Med. 26 (2015) 103.

[219] Z. Zhang, P. Sharma, C. N. Borca, P. A. Dowben, A. Gruverman, Polarization-specific adsorption of organic molecules on ferroelectric $LiNbO_3$ surfaces, Appl. Phys. Lett. 97 (2010) 243702.

[220] H. J. Seo, Y. E. Cho, K. Taewan, H. I. Shin, I. S. Kwun, Zinc may increase bone formation through stimulating cell proliferation, alkaline phosphatase activity and collagen synthesis in osteoblastic MC3T3-E1 cells, Nutri. Res. Pract. 4 (2010) 356-361.

[221] B. A. Dikici, S. Dikici, O. Karaman, H. Oflaz, The effect of zinc oxide doping on mechanical and biological properties of 3D printed calcium sulfate based scaffolds, Biocybernetics and Biomedical Engineering 37 (2017) 733-741.

[222] B. K. Shrestha, S. Shrestha, A. P. Tiwari, J. I. Kim, S. W. Ko, H. J. Kim, C. H. Park, C. S. Kim Bio-inspired hybrid scaffold of zinc oxide-functionalized multi-wall carbon nanotubes reinforced polyurethane nanofibers for bone tissue engineering, Mater. Des. 133 (2017) 69-81.

[223] B. Felice, M. A. Sanchez, S. C. Socci, L. D. Sappia, M. I. Gomez, M. K. Cruz, C. J. Felice, M. Marti, M. I. Pividori, G. Simonelli, A. P. Rodriguez, Controlled degradability of PCL-ZnO nanofibrous scaffolds for bone tissue engineering and their antibacterial activity, Mater. Sci. Eng. C. 93 (2018) 724-738.

[224] S. M. Nakhmanson, A. Calzolari, V. Meunier, J. Bernholc, M. Buongiorno Nardelli, Spontaneous Polarization and Piezoelectricity in Boron Nitride Nanotubes, Physical Review B. 67 (2003) 235406.

[225] C. Zhi, Y. Bando, C. Tang, D. Golberg, Immobilization of proteins on boron nitride nanotubes, J. Am. Chem. Soc. 127 (2005) 17144-17145.

[226] C. Shuai, Z. Han, P. Feng, C. Gao, T. Xiao, S. Peng, Akermanite scaffolds reinforced with boron nitride nanosheets in bone tissue engineering, J. Mater. Sci. Mater. Med. 26 (2015) 188.

[227] S. Nagarajan, H. Belaid, C. Pochat-Bohatier, C. Teyssier, I. Iatsunskyi, E. Coy, S. Balme, D. Cornu, P. Miele, N. S. Kalkura, V. Cavailles, M. Bechelany, Design of Boron Nitride/Gelatin Electrospun Nanofibers for Bone Tissue Engineering, ACS Appl. Mater. Inter. 9 (2017) 33695-33706.

[228] E. Fukada, T. Sakurai, Piezoelectricity in Polarized Poly(vinylidene fluoride) Films, Polym. J. 2 (1970) 656-662.

[229] D. M. Correia, R. Gonçalves, C. Ribeiro, V. Sencadas, G. Botelho, J. L. G. Ribelles, S. L. Mendez, Electrosprayed poly(vinylidene fluoride) microparticles for tissue engineering applications, RSC Adv. 4 (2014) 33013-33021.

[230] C. Frias, J. Reis, F. Capela e Silva, J. Potes, J. Simões, A. T. Marques, Polymeric piezoelectric actuator substrate for osteoblast mechanical stimulation, Journal of Biomechanics 43 (2010) 1061-1066.

[231] C. Ribeiro, S. Moreira, V. Correia, V. Sencadas, J. G. Rocha, F. M. Gama, J. L. G. Ribelles, S. L. Mendez, Enhanced proliferation of preosteoblastic cells by dynamic piezoelectric stimulation, RSC Adv. 2 (2012) 11504-11509.

[232] C. Ribeiro, J. A. Panadero, V. Sencadas, S. L. Mendez, M. N. Tamano, D. Moratal, M. S. Sanchez, J. L. G. Ribelles, Fibronectin adsorption and cell response on electroactive poly(vinylidene fluoride) films, Biomed. Mater. 7 (2012) 035004.

[233] S. M. Damaraju, S. Wu, M. Jaffe, T. L. Arinzeh, Structural changes in PVDF fibersdue to electrospinning and its effect on biological function, Biomed. Mater. 8 (2013) 045007.

[234] R. S. Almeida, M. T. Machiavello, E. Carvalho, L. Cordón, S. Doria, L. Senent, D. Correia, C. Ribeiro, S. L. Mendez, R. Sabater I. Serra, J. G. Ribelles, A. Sempere, Human Mesenchymal Stem Cells Growth and Osteogenic Differentiation on Piezoelectric Poly(vinylidene fluoride) Microsphere Substrates, Int. J. Mol. Sci. 18 (2017) 2391.

[235] J. Parssinen, H. Hammaren, R. Rahikainen, V. Sencadas, C. Ribeiro, S. Vanhatupa, S. Miettinen, S. Lanceros-Mendez, V. P. Hytonen, Enhancement of adhesion and promotion of osteogenic differentiation of human adipose stem cells by poled electroactive poly(vinylidene fluoride), J. Biomed. Mater. Res. A 103 (2015) 919-928.

[236] C. Ribeiro, J. Parssinen, V. Sencadas, V. Correia, S. Miettinen, V. P. Hytonen, S. Lanceros-Méndez, Dynamic piezoelectric stimulation enhances osteogenic differentiation of human adipose stem cells, J. Biomed. Mater. Res. A 103 (2015) 2172-2175.

[237] M. T. Rodrigues, M. E. Gomes, J. F. Mano, R. L. Reis, β-PVDF Membranes Induce Cellular Proliferation and Differentiation in Static and Dynamic Conditions, Mater. Sci. Forum 587-588 (2008) 72-76.

[238] H. Tamai, K. Igaki, E. Kyo, K. Kosuga, A. Kawashima, S. Matsui, H. Komori, T. Tsuji, S. Motohara, H. Uehata, Initial and 6-month results of biodegradable poly-l-lactic acid coronary stents in humans, Circulation, 102 (2000) 399-404.

[239] N. Barroca, P. M. Vilarinho, A. L. Daniel-Da-Silva, A. Wu, M. H. Fernandes, A. Gruverman, Protein adsorption on piezoelectric poly(L-lactic) acid thin films by scanning probe microscopy, Appl. Phys. Lett. 98 (2011) 133705.

[240] E. J. Bergsma, F. R. Rozema, R. R. Bos, W. C. Debruijn, Foreign body reaction to resorbable poly(L-lactic) bone plates and screws used for the fixation of unstable zygomatic fractures, J Oral Maxillofac Surg 51 (1993) 666-670.

[241] J. C. Middleton, A. J. Tipton, Synthetic biodegradable polymers as orthopedic devices, Biomaterials 21 (2000) 2335-2346.

[242] M. Esmaeili, M. S. Baei, Fabrication of biodegradable polymer nanocomposite from copolymer synthesized by C. necator for bone tissue engineering, World Appl. Sci. J. 14 (2011) 106-111.

[243] Y. Ando, E. Fukada, Piezoelectric properties and molecularmotion of poly*β*-hydroxybutyrate) films, J. Polym. Sci. Polym. Phys. 22 (1984) 1821-1834.

[244] E. Fukada, History and recent progress in piezoelectric polymers, IEEE Trans. Ultrason. Ferroelec. Freq. Control 47 (2000) 1277-1290.

[245] Y. Wang, Q. Wu, G. Chen, Attachment, proliferation and differentiation of osteoblasts on random biopolyester poly(3-hydroxybutyrate-co-3-hydroxyhexanoate) scaffolds, Biomaterials 25 (2004) 669-675.

[246] Y. Wang, Q. Wu, J. Chen, G. Chen, Evaluation of three-dimensional scaffolds made of blends of hydroxyapatite and poly(3-hydroxybutyrate-co-3-hydroxyhexanoate) for bone reconstruction, Biomaterials 26 (2005) 899-904.

[247] E. I. Pascu, J. Stokes, G. B. McGuinness, Electrospun composites of PHBV, silk fibroin and nano-hydroxyapatite for bone tissue engineering, Mater. Sci. Eng. C 33 (2013) 4905-4916.

[248] J. Ni, M. Wang, *In vitro* evaluation of hydroxyapatite reinforcedpolyhydroxybutyrate composite, Mater. Sci. Eng. C 20 (2002) 101-109.

[249] J. Xi, L. Zhang, Z. Zheng, G. Q. Chen, Preparation and evaluation of porous poly (3-hydroxybutyrate-co-3-hydroxyhexanoate)-hydroxyapatite composite scaffolds, J. Biomat. Appl. 22 (2008) 293-307.

[250] L. P. Wu, M. You, D. Wang, G. Peng, Z. Wang, G. Q. Chen, Fabrication of carbon nanotube (CNT)/poly(3- hydroxybutyrate-co-3-hydroxyhexanoate) (PHBHHx) nanocomposite films for human mesenchymal stem cell (hMSC) differentiation, Polym. Chem. 4 (2013) 4490-4498.

[251] E. Fukada, I. Yasuda, Piezoelectric Effects in Collagen, Jpn. J. Appl. Phys. 3 (1964) 117-121.

[252] D. Puppi, F. Chiellini, A. M. Piras, E. Chiellini, Polymeric materials for bone and cartilage repair, Progr. Poly. Sci. 35 (2010) 403-440.

[253] N. E. Adel Elkasabgy, A. A. Mahmoud, R. N. Shamma, Determination of Cytocompatability and Osteogenesis Properties of in-Situ forming Collagen Based Scaffolds Loaded with Bone Synthesizing Drug for Bone Tissue Engineering, Internat. J. Poly. Mater. Poly, Biomaterials 67 (2017) 494-500.

[254] P. Angele, J. Abke, R. Kujat, H. Faltermeier, D. Schumann, M. Nerlich, B. Kinner, C. Englert, Z. Ruszczak, R. Mehri, R. Mueller, Influence of different collagen species on physicochemical properties of crosslinked collagen matrices, Biomaterials 25 (2004) 2831-2841.

[255] B. Sugarman, E. J. Young, Infections associated with prosthetic devices: magnitude of the problem, Infect. Dis. Clin. N. Am. 3 (1989) 187-199.

[256] R. H. Jr Fitzgerald, Infections of hip prostheses and artificial joints, Infect. Dis. Clin. N. Am. 3 (1989) 329–338.

[257] J. W. Costerton, P. S. Stewart, E. D. Greenberg, Bacterial biofilms: a common cause of persistent infections, Science 284 (1999) 1318-1322.

[258] E. F. Berbari, A. D. Hanssen, M. C. Duffy, J. M. Steckelberg, D. M. Ilstrup, W. S. Harmsen, D. R. Osmon, Risk Factors for Prosthetic Joint Infection: Case-Control Study, Clin. Infect. Dis. 27 (1998) 1247-1254.

[259] A. Singh, A. Dubey, Various biomaterials and techniques for improving antibacterial response, ACS Appl. Bio Mater. 1 (2018) 3-20.

[260] R. E. Baier, A. E. Meyer, J. R. Natiella, R. R. Natiella, J. M. Carter, Surface properties determine bioadhesive outcomes: methods and results, J Biomed Mater Res 18 (1984) 327-355 0021-9304.

[261] J.-I. Flock, Extracellular-matrix-binding proteins as targets for the prevention of Staphylococcus aureus infections, Molecular medicine today, 5 (2000) 532-537.

[262] M. Roy, J. S. Somerson, K. Kerr, J. L. Conroy (March 23rd 2012), Pathophysiology and Pathogenesis of Osteomyelitis, Osteomyelitis, (2012).

[263] B. D. Hoyle, J. W. Costerton, Bacterial resistance to antibiotics: the role of biofilms, Prog Drug Res, 37 (1991) 91-105.

[264] P. S. Stewart, J. Costerton, Antibiotic resistance of bacteria in biofilms, The Lancet 358(2001) 135-138.

[265] R. M. Donlan, J. W. Costerton, Biofilms: Survival mechanisms of clinically relevant microorganisms, Clin. Microbiol. Rev. 15 (2002) 167-193.

[266] M. K. Dasgupta, P. Zuberbuhler, A. Abbi, F. L. Harley, N. E. Brown, K. Lam, J. B. Dossetor, J. W. Costerton, Combined evaluation of circulating immune complexes and antibodies to Pseudomonas aeruginosa as an immunologic profile in relation to pulmonary function in cystic fibrosis, J Clin Immunol. 7 (1987) 51-58.

[267] J. W. Costerton, K. J. Cheng, G. G. Geesey, T. I. Ladd, J. C. Nickel, M. Dasgupta, T. J. Marrie, Bacterial biofilms in nature and disease, Annu. Rev. Microbiol. 41(1987) 435-464.

[268] K. L. Menzies, L. W. Jones, The Impact of Contact Angle on the Biocompatibility of Biomaterials, Optometry and Vision Science, 87 (2010) 387-399.

[269] S. Baron, Medical Microbiology, University of Texas Medical Branch, Galveston, Tex, USA, 4th edition, (1996).

[270] A. Wright, D. J. Tipper, The outer membrane of gram-negative bacteria, p. 427, In Sokatch JR, Ornston LN (eds): The bacteria. Vol. 7, Academic Press, San Diego, (1979).

[271] F. G. Ferris, T. J. Beveridge, Site specificity of metallic ion binding in Escherichia coli K-12 lipopolysaccharide, Can. J. Microbiol. 32 (1986) 52-55.

[272] M. Rivera, E. J. McGroarty, Analysis of a common antigen lipopolysaccharide from Pseudomonas aerugenosa, J. Bacteriol. 171 (1989) 2244-2248.

[273] R. Sonohara, N. Muramatsu, H. Ohshima, T. Kondo, Difference in surface properties between Escherichia coli and Staphylococcus aureus as revealed by electrophoretic mobility measurement, Biophys. Chem. 55 (1995) 273-277.

[274] E. Kłodzińska, M. Szumski, E. Dziubakiewicz, K. Hrynkiewic, E. Skware, W. Janusz, B. Buszewsk, Effect of zeta potential value on bacterial behavior during electrophoretic separation, Electrophoresis, 31(2010) 1590-1596.

[275] T. Nakahara, H. Yaguchi, M. Yoshida, J. Miyakoshi, Effects of exposure of CHO-K1Cells to a 10-T static magnetic field, Radiology 224 (2002) 817-822.

[276] I. Bajpai, N. Saha, B. Basu, Moderate intensity static magnetic field has bactericidal effect on E. coli and S. epidermidis on sintered hydroxyapatite, J. Biomed. Mater. B: Appl. Biomat. 100B (2012) 1206-1217.

[277] I. Bajpai, K. Balani, B. Basu, Synergistic effect of static magnetic field and HA-Fe3O4 magnetic composites on viability of S. aureus and E. coli bacteria, J. Biomed. Mat. Res. B: Appl. Biomat.102B (2014) 524-532.

[278] W. K. Liu,M. R. Brown, T. S. Elliott, Mechanisms of the bactericidal activity of low amperage electric current (DC). J Antimicrob. Chemother. 39 (1997) 687-695.

[279] S. Boda, I. Bajpai, B. Basu, Inhibitory effect of direct electric field and HA-ZnO composites on S. aureus biofilm formation, J. Biomed. Mat. Res. Part B: Appl. Biomat. 104 (2015)1064-1075.

[280] G. Tan, S. Wang, Y. Zhu, L. Zhou, P. Yu, X. Wang, T. He, J. Chen, C. Mao, C. Ning, Surface-Selective Preferential Production of Reactive Oxygen Species on Piezoelectric Ceramics for Bacterial Killing, ACS appl. Mat. Interf. 8 (2016) 24306-24309.

[281] A. Singh, K. Reshma, A. K. Dubey, Combined effect of surface polarization and ZnO addition on antibacterial and cellular response of Hydroxyapatite-ZnO composites, Materials Science and Engineering: C, 107 (2020) 110363.

[282] S. Swain, R. N. Padhy, T. R. Rautray, Polarized piezoelectric bioceramic composites exhibit antibacterial activity, Materials Chemistry and Physics, 239 (2020) 122002.

[283] A. S. Verma, A. Sharma, A. Kumar, A. Mukhopadhyay, D. Kumar and A. K. Dubey, Multifunctional response of piezoelectric sodium potassium niobate (NKN) toughened hydroxyapatite based biocomposites, ACS Appl. Bio. Mat. 2020, DOI: 10.1021/acsabm.0c00642.

[284] A. S. Verma, A. Singh, D. Kumar and A. K. Dubey, Electro-mechanical and Polarization-Induced Antibacterial Response of 45S5 Bioglass-Sodium Potassium Niobate Piezoelectric Ceramic Composites. ACS Biomaterials Science & Engineering, 6 (2020) 3055-3069.

[285] M. Kalbacova, S. Roessler, U. Hempel, R. Tsaryk, K. Peters, D. Scharnweber, J. C. Kirkpatrick, P. Dieter, The Effect of Electrochemically Simulated Titanium Cathodic Corrosion Products on ROS Production and Metabolic Activity of Osteoblasts and Monocytes/macrophages. Biomaterials, 28(2007) 3263-3272.

[286] E. Serena, E. Figallo, N. Tandon, C. Cannizzaro, S. Gerecht, N. Elvassore, G. Vunjak-Novakovic, Electrical Stimulation of Human Embryonic Stem Cells: Cardiac Differentiation and the Generation of Reactive Oxygen Species, Exp. Cell. Res. 315(2009) 3611-3619.

[287] S. Kumar, R. Vaish, S. Powar, Surface-selective bactericidal effect of poled ferroelectric materials, J. Appl. Phys. 124 (2018) 014901.

[288] G. Harkes, J. Feijen, J. Dankert, Adhesion of Escherichia coli on to a series of poly(methacrylates) differing in charge and hydrophobicity, Biomaterials, 12(1991) 853-860.

[289] L. Kodjikian, C. Burillon, C. Roques, G. Pellon, J. Freney, F. N. Renaud, Bacterial adherence of *Staphylococcus epidermidis* to intraocular lenses: a bioluminescence and scanning electron microscopy study, Invest. Ophthalmol. Vis. Sci. 44(2003) 4388-4394.

[290] M. Henriques, C. Sousa, M. Lira, M. Elisabete, R. Oliveira, J. Azeredo, Adhesion of *Pseudomonas aeruginosa* and *Staphylococcus epidermidis* to silicone-hydrogel contact lenses, Optom. Vis. Sci. 82(2005) 446-450.

[291] A. Okada, T. Nikaido, M. Ikeda, K. Okada, J. Yamauchi, R. M. Foxton, H. Sawada, J. Tagami, K. Matin, Inhibition of biofilm formation using newly developed coating materials with self-cleaning properties, Dent. Mater. J.27 (2008) 565-572.

[292] R. A. MacLeod, E. E. Snell, The effect of related ions on the potassium requirement of lactic acid bacteria, J. Biol. Chem.176 (1948) 39-52.

[293] K. Dawson, J. Boling, Effects of potassium ion concentrations on the antimicrobial activities of ionophores against ruminal anaerobes, Appl. Environ. Microb. 53 (1987) 2363-2367.

[294] N. Niño-Martínez, M. F. S. Orozco, G.-A. Martínez-Castañón, F. T. Méndez, F. Ruiz, Molecular mechanisms of bacterial resistance to metal and metal oxide nanoparticles, Int. J. Mol. Sci. 20 (2019) 2808.

[295] A. Q. Hou, G. C. Feng, J. Y. Zhuo, G. Sun, UV Light-Induced Generation of Reactive Oxygen Species and Antimicrobial Properties of Cellulose Fabric Modified by 3,3 ′,4,4 ′-Benzophenone Tetracarboxylic Acid, ACS Appl. Mater. Interf. 7(2015) 27918-27924.